Fermi National Accelerator Laboratory

FERMILAB-Conf-82/55-THY
September, 1982

A THOUSAND TeV IN THE CENTER OF MASS: INTRODUCTION TO HIGH ENERGY STORAGE RINGS+

J.D. Bjorken

Fermi National Accelerator Laboratory
P.O. Box 500
Batavia, Illinois 60510

I. INTRODUCTION

These lectures must begin with an apology. Normally at schools such as this, one expects the lecturer to be an acknowledged expert on the subject matter he is discussing. Here this is not the case. Design of high energy proton storage rings is not exactly my forte. Why am I doing this? There are several reasons, short of mental illness.*

1. I want to learn this subject myself and there is no better way than trying to teach it. And Ferbel didn't stop me.

2. There needs to be a broader knowledge of accelerator physics in the elementary-particle community. Experimentalists at the storage rings find themselves especially closely coupled to their machine and its operation. And theorists can find interesting and challenging questions which lie at the frontier of the very active field of nonlinear mechanics.

3. Straightforward extrapolation of existing acceleration techniques would seem to lead to very large, expensive machines. While we may envision one, perhaps two generations of future accelerators using essentially existing techniques, the question of how to go beyond that is a difficult one. There seems to be a growing feeling that it is not too soon to start to face up to the problem. A look at the alternative--as we do here--can only provide stimulation.

*See Appendix II.

+Lectures given at the 1982 NATO Advanced Study Institute, Lake George, N. Y., June 1982.

Operated by Universities Research Association Inc. under contract with the United States Department of Energy

There is a famous plot ("Livingston Plot") of cms energy attained as a function of calendar year (Fig. 1). One sees, remarkably, a doubling-time of ~2-3 years. Can this be maintained? Extrapolating into the future, there exists UNK, the Soviet project, talk of a VBA (very big accelerator) with $E_{cms} \lesssim 50$ TeV (for colliding beams), and even the beginnings of discussion of a possible US machine on that energy scale.[1] Beyond that lies unknown territory, and a fundamental challenge to the natural push to even higher energy. This unknown territory of the distant future is where we shall reside during these lectures. We shall project ourselves into the years 2010-2020, and look[2] at an utterly unimaginative scaled up $p\bar{p}$ collider of 500 TeV + 500 TeV. Needless to say, such a machine is clumsy (circumference $> 10^3$km) and expensive (cost > 1000 Tevatrons) and must not be taken seriously. Nevertheless, the choice has the following advantages:

1. By stretching present ideas to (beyond?) the breaking point, we learn the scaling laws for more practical machines, i.e. how machine parameters scale with energy.

2. Once having grappled with such staggering energy scales, it is easier to interpolate back to "reasonable" (??) machines like the VBA.

3. It is an interesting exercise to see whether such a machine, even were it economically feasible, could work, or whether there are intrinsic technical limits to the energy-scale available to the present technology.

4. A 500 TeV proton ring is a nice pedagogical machine. In particular, synchrotron-radiation becomes quite important, and thus this proton machine shares features--and problems--characteristic of contemporary e^+e^- storage rings.

5. The machine is so big, so remote in time, and so unlikely to be built that no one could be misled into thinking that I take any of this seriously. To repeat, this machine is not to be taken seriously. <u>This machine is not to be taken seriously.</u> <u>THIS MACHINE IS NOT TO BE TAKEN SERIOUSLY.</u>

Our main purpose, after all, is pedagogy. In the next section, we shall try to outline in a rough semiquantitative way the big picture, i.e., we try to provide an overview of the material to follow. Section III is devoted to a more detailed discussion of linear optics and betatron motions. In Section IV we briefly survey questions of errors, tolerances and nonlinear resonances. In Section V we provide a very sketchy parameter list for the 500 TeV collider, and discuss some of the uncertainities. Section VI discusses some of the various demands upon the detection apparatus--especially the apparent inevitability of multiple interactions per bunch crossing. Section VII is devoted to concluding comments. An appendix provides a bibliography from which these lectures where prepared.

II. OVERVIEW

This section is divided into the following subsections:

1. Closed orbit
2. Vertical motion (betatron oscillations)
3. Horizontal motion (betatron oscillations and momentum dispersion)
4. Synchrotron radiation
5. Longitudinal phase space
6. Synchrotron damping of the phase space
7. Quantum excitation of the phase space.
8. Single beam instabilities
9. Luminosity
10. Beam-beam effect

1. Closed Orbit

Get a map and draw a circle. (This is a common pastime of laboratory directors.[3]) The bending radius ρ is proportional to momentum p and inversely proportional to magnetic field B:

$$p = eB\rho \tag{2.1}$$

The conversion factor is

$$0.3 \text{ GeV/c} = 1 \text{ T-m} = 10 \text{ kG-m} \tag{2.2}$$

(We shall often set $\hbar = c = 1$.) We shall choose 10T magnets, inasmuch as that has already been projected for the 20 TeV VBA. This gives for nominal radius ρ and circumference C:

$$\begin{aligned} \rho &= 170 \text{ km.} \\ C &= 1100 \text{ km.} \end{aligned} \tag{2.3}$$

The actual values will be somewhat larger in order to account for the quadrupole magnets and straight sections.

2. Vertical Motion

No particle exactly follows the design orbit. The typical particle undergoes small oscillations about the design orbit. To a good approximation the vertical, horizontal, and longitudinal motions may be treated independently. Focussing is provided by quadrupole magnets; we write (with z the vertical coordinate and x the horizontal coordinate transverse to the direction of motion)

$$B_x = Gz \tag{2.4}$$

(implying, via Maxwell equations, B_z=+Gx, i.e. defocussing in the horizontal plane.)

The state-of-the-art maximum gradient G is ~1 T/cm; we take

$$G \simeq 2T/cm. \tag{2.5}$$

The transverse kick a particle gets in going through a quadrupole magnet of length ℓ is roughly

$$\Delta p_x \cong eG\ell z \tag{2.6}$$

For focussing in both planes one alternates focussing and defocussing quadrupoles which are spaced in such a way that, on average, the $<|z|>$ of particles at defocussing quads is smaller that the $<|z|>$ at focussing quads. Provided this can be arranged, then there will be net focussing. The condition for this is, in order of magnitude, that the focal length f of the quads be comparable to their spacing L. A typical particle orbit then is shown in Fig. 2.

From the above equation we see this implies

$$\theta_z \sim \frac{z}{f} \sim \frac{\Delta p_z}{p} \sim \frac{eG\ell z}{p} \tag{2.7}$$

Thus the condition for stable, strong focussing is

$$eG\ell L \sim p = eB\rho \tag{2.8}$$

Normal economics implies that the investment in quads not be a large perturbation on the investment in dipole magnets

$$\frac{\ell}{L} \lesssim (0.1\text{-}0.2) \tag{2.9}$$

and hence

$$0.1eG\ell^2 \sim p = eB\rho \tag{2.10}$$

The spacing between F and D quads is then

$$L \sim 3\sqrt{\frac{B\rho}{G}} \tag{2.11}$$

and (for fixed magnet parameters) scales as $E^{1/2}$. We estimate

	Estimated	Actual		
$L \sim$	20 m	30 m	Fermilab TeVatron	(2.12)
	500 m	(400 m)	2020 Machine	

The wavelength of the betatron oscillations evidently also scales with L; actually the typical wave-number is $\sim L^{-1}$. A very fundamental machine parameter is the tune. It is defined as the number of betatron oscillations per revolution

$$\nu_z = \frac{\text{Circumference}}{\text{Betatron wavelength}} \sim \frac{2\pi\rho}{2\pi L} \sim \frac{\rho}{L} \tag{2.13}$$

We see that the tune also scales as $\sim E^{1/2}$. We find from the rough estimate

	Estimated	Actual		
$\nu_z \sim$	50	19.3	TeVatron	(2.14)
	350	(400)	2020 Machine	

(The discrepancy in the case of the TeVatron is accounted for by a smaller value of ℓ/L and a larger choice of betatron wavelength $\simeq 10L$.)

It is useful to consider the beam as a population in phase space. Vertical phase-space* is just z-p_z space. Provided the

*Canonical phase space here: the definition typically used by accelerator physicists contains a factor γ; cf Chapter III.

dynamics is derivable from a Hamiltonian (as is the case for particles moving in external electromagnetic fields--including time-dependent fields), the area in phase-space must be conserved, according to the Liouville theorem. Typically this area, as determined essentially by the low energy source, is

$$\Delta z \, \Delta p_z = \text{phase-space area} \simeq 1 \text{ MeV-cm}. \tag{2.15}$$

(In natural units this is $\sim 10^{10}\hbar$.)

We may now estimate the nominal beam size in a storage ring. Our previous estimate in Eqn. (2.6) relates Δp_z to Δz through the focal structure of the lattice (by <u>lattice</u> we mean the array of magnets comprising the ring)

$$\Delta p_z \sim eG\ell \, \Delta z \tag{2.16}$$

Then

$$\Delta z \, \Delta p_z \sim \frac{eG\ell}{L} \cdot [L(\Delta z)^2] \tag{2.17}$$

Only the right-hand factor is not a fixed quantity. Hence the nominal beam size* scales as

$$\Delta z \sim L^{-1/2} \sim E^{-1/4} \tag{2.18}$$

The nominal transverse momentum in the beam scales as

$$\Delta p_z \sim E^{1/4} \tag{2.19}$$

Putting in the numbers gives

	TeVatron	2020 Machine
$\Delta z \sim$	0.3 mm	70μ
$\Delta p_z \sim$	30 MeV	140 MeV

(2.20)

The shape of the population in phase space changes as one proceeds around the ring. It is typically elliptical, but the axes and orientation (but <u>not</u> area!) vary as one proceeds around the ring, as shown in Fig. 3.

*This $E^{-1/4}$ scaling of beam size in different storage rings should not be confused with the change in beam-size during acceleration. There the gradient G scales with B and hence with energy in order to keep a constant tune ν during the acceleration cycle. Therefore during acceleration, $\Delta z \sim E^{-1/2}$; $\Delta p_z \sim E^{+1/2}$.

3. Horizontal Motion

The description of horizontal betatron oscillations is very similar to vertical oscillations. Inclusion of the effect of curvature of the design orbit changes the tune ν_x by a negligible amount. A more important effect has to do with dispersion: an off-momentum particle has a different closed orbit (cf Fig. 4). If the momentum exceeds the design momentum by an amount Δp (in the high energy limit), the new closed orbit will lie at larger radius. Write, for a typical particle

$$x(s) = x_\varepsilon(s)+x_\beta(s) \tag{2.21}$$

where x_β is the betatron amplitude at coordinate s along the design orbit, and x_ε is the correction to the radius of the closed orbit. In linear approximation

$$x_\varepsilon = \eta(s)\frac{\Delta p}{p} \tag{2.22}$$

Let us estimate the nominal value of $\eta(s)$. In going through a cell (a cell is the basic element of the lattice consisting of F quad, D quad and the two sets of intermediate bending magnets), the off-momentum particle must be bent through the same angle; hence it must get an extra p_T kick from the quadrupoles in proportion to its momentum deviation $\Delta p/p$. We must have

$$\frac{\Delta p_{||}}{p_{||}} \sim \frac{\text{Extra } p_T \text{ kick}}{\text{Main } p_T \text{ kick}} = \frac{eG\ell x_\varepsilon}{2eBL} \tag{2.23}$$

This implies

$$\langle\eta(s)\rangle \sim \frac{2B}{G}\,\frac{L}{\ell} \tag{2.24}$$

a value independent of machine energy. Putting in the numbers gives

	Estimated	Actual	
$\langle\eta(s)\rangle \sim$	m	2 m	TeVatron
	1 m	0.7 m	2020 Machine

(2.25)

For typical machine apertures of a few centimeters, a momentum spread $\Delta p/p \lesssim 10^{-2}$-$10^{-3}$ may be accepted independent of energy. The actual momentum spread in the beam must be found by considering longitudinal phase-space. We do this in part 5.

4. Synchrotron Radiation

In proton storage rings the beam may be bunched as it is during acceleration or as in $p\bar{p}$ colliders such as TeV I, where $\bar{p}$'s are in short supply. In other cases the beam may be unbunched ("coasting") as in the CERN ISR (or as in the ISABELLE design). In e^+e^- machines, the beams are necessarily bunched, because the energy loss from synchrotron radiation must be compensated by an RF accelerating system. In our 500 TeV machine, protons also emit a significant amount of synchrotron radiation. The handbook formula[4] for the energy loss per turn is (with $\hbar=c=1$)

$$\text{Energy loss/revolution} \equiv U_0 = \frac{4\pi\alpha}{3\rho}\left(\frac{E}{m}\right)^4 \tag{2.26}$$

With our parameters, this implies

$$U_0 \sim 3 \text{ GeV/turn} \tag{2.27}$$

This radiation is emitted in a broad spectrum of photon energies, but the typical photon energy or critical energy E_c is given by

$$E_c \sim \frac{3}{\rho}\left(\frac{E}{m}\right)^3 \sim \frac{9U_0}{4\pi\alpha}\cdot\frac{m}{E} \tag{2.28}$$

For the 2020 machine, this is

$$E_c \sim 300 \text{ keV} \tag{2.29}$$

This gives the typical number of photons emitted per turn as

$$\text{Photons/revolution} \sim \frac{U_0}{E_c} \sim \frac{\gamma}{137} \tag{2.30}$$

At 500 TeV, we get

$$\text{Emitted photons/revolution} \sim 4\times10^3 \tag{2.31}$$

Thus a coasting proton would lose ≈1% of its energy in 2000 revolutions. Inasmuch as the revolution frequency is 250 Hz, 2000 turns is only 8 sec. A coasting beam is not possible. An RF system must be provided.

5. Longitudinal Phase Space

To define longitudinal coordinates, we may use the energy deviation ε (or momentum deviation $\Delta p \approx \varepsilon$) and the distance Δs from a reference particle at the center of the bunch (or equivalently the arrival-time delay $(-\tau)$ of the particle at a given point of observation). As one might expect, ε and τ (or Δp and Δs) are canonically conjugate variables. Somewhere around the ring RF cavities must be placed to provide the acceleration. A particle with energy E entering the cavity at time τ leaves the cavity with energy $E+V(\tau)$, where by definition this defines the RF voltage $V(\tau)$. The RF voltage must be synchronous with the particle motion around the machine. Thus $V(\tau)$ must be periodic

$$V(\tau) = V\left(\tau + \frac{2\pi}{h\omega_0}\right) \tag{2.32}$$

where

$$f_0 = \frac{\omega_0}{2\pi} = \text{revolution frequency} \tag{2.33}$$

and

$$h = \text{integer} \equiv \text{harmonic number} \tag{2.34}$$

Typically (but not always) $V(\tau)$ is sinusoidal, and we shall assume it to be true here:

$$V(\tau) = V_0 \sin\left(h\omega_0\tau + \phi_0\right) \tag{2.35}$$

The choice of RF frequency is determined in large part by practical considerations beyond the scope of these lectures. At Fermilab, the RF frequency is ~50 Mhz; at CERN it is ~200 Mhz. The higher the frequency, the less bulky the cavities, and we shall provisionally pick (rather arbitrarily*) a frequency of 500 Mhz. This gives the harmonic number

$$h \sim 2\times10^6 \tag{2.36}$$

The synchronous particle $(\tau=0)$ will gain energy $V_0 \sin \phi_0$ per turn. This must match the energy loss U_0:

*In retrospect, I think this is a mistake. Lower frequency seems preferable.

$$U_0 = V_0 \sin \phi_0 \tag{2.37}$$

We may now write down equations of motion for ε and τ, which may be functions of time. The time variation is assumed to be slow compared to the revolution frequency. Then we have

$$\frac{d\varepsilon}{dt} = \frac{\omega_0}{2\pi} \left[V_0 \sin(h\omega_0\tau+\phi_0)-U_0-\frac{\partial U_0}{\partial E}\,\varepsilon\right] \tag{2.38}$$

(The last term ultimately must be included. It provides damping; here we temporarily ignore it.)

Even in the absence of RF, the variable τ will change with time if the particle has a momentum error. This occurs because the revolution frequency depends upon momentum. We write

$$\frac{\Delta\omega_0}{\omega_0} = -\frac{\Delta T}{T} \equiv \eta\,\frac{\Delta p}{p} \tag{2.39}$$

where the "dilation factor" or "momentum-compaction" η is not the same $\eta(s)$ as introduced in connection with the dispersion. However this η (sometimes called α_p) is related to $\eta(s)$. At high energy,* evidently

*At lower energy, there is another contribution to η (of opposite sign) coming from the change in velocity with momentum. Since

$$\frac{\Delta T}{T} = \frac{\Delta\rho}{\rho} - \frac{\Delta v}{v} \tag{F.1}$$

and $\Delta v/v \simeq \gamma^{-2}(\Delta p/p)$, we get

$$\eta = \frac{\langle\eta(s)\rangle}{\rho} - \frac{1}{\gamma^2} \equiv \frac{1}{\gamma_T^2} - \frac{1}{\gamma^2} \tag{F.2}$$

At the value $\gamma=\gamma_T$, or transition energy, η changes sign and longitudinal motion becomes more nontrivial. This creates some complication during acceleration in lower energy machines. From Eqns (2.8), (2.13), and (2.24), we may see that $\gamma_T \simeq \nu$. For the 2020 machine, injection energy will be well above transition.

$$\eta \frac{\Delta p}{p} = \frac{<\Delta\rho>}{\rho} = \frac{<\eta(s)>}{\rho} \frac{\Delta p}{p} \tag{2.40}$$

or

$$\eta = \frac{<\eta(s)>}{\rho} \tag{2.41}$$

For the 2020 machine, our rough estimate gives,

$$\eta \sim 6\times 10^{-6} \tag{2.42}$$

Because of the dispersion, an off-energy particle will, in absence of other effects, change its position Δs, (or time τ) relative to the reference particle. We have

$$\frac{d\tau}{dt} = -\eta\frac{\Delta p}{p} \equiv -\frac{\eta}{E}\,\varepsilon \tag{2.43}$$

This, together with Eqns. (2.37) and (2.38), leads to the equation of motion

$$\frac{d^2\tau}{dt^2} = -\frac{\eta}{E}\,\frac{\omega_0}{2\pi}\,V_0[\sin(h\omega_0\tau+\phi_0)-\sin\phi_0] \tag{2.44}$$

For $\phi_0=0$ (no synchrotron radiation) this is the equation of a pendulum, with τ playing the role of an angle ("synchrotron phase"). For small amplitudes there is stability; for large amplitudes there is not, and τ on average increases linearly with time.

For nonvanishing ϕ_0, there is again phase-stability for small amplitudes. For large amplitudes τ increases (on average) quadratically with time, and consequently ε increases linearly with time, implying eventual loss of the particle.

In the limit of small τ, Eqn (2.44) is just an oscillator equation, and the angular frequency Ω_s (synchrotron frequency) is

$$\frac{\Omega_s}{\Omega_0} = \left(\frac{\eta h V_0 \cos\phi_0}{2\pi E}\right)^{1/2} \tag{2.45}$$

For our 500 TeV machine, we get (choosing $V_0 \sim 5$ GeV) for the frequency of synchrotron oscillations,

$$\frac{\Omega_s}{2\pi} \sim 1 \text{ Hz} \tag{2.46}$$

justifying a posteriori our assumption of slow variation of τ with time.

It is again important to view all this in the longitudinal phase space. Considering first the case $\phi_0=0$, we see that in ε-τ space the small amplitude orbits are approximately circular (or elliptical), centered at $\tau=0$, $\pm 2\pi/h\omega_0$, $\pm 4\pi/h\omega_0$, (Fig. 5). Very large amplitude orbits are straight lines $\varepsilon \approx$ const. In between is a special orbit, the separatrix, which comprises the boundary between oscillatory and non-oscillatory motion (it corresponds to the pendulum oscillation with $\pm 180°$ excursion in angle). The equation for the separatrix is easily worked out, especially if one remembers the facts of life about pendula. The region in phase space of oscillatory motion which is enclosed by the separatrix is called, for obscure historical reasons, an RF bucket. The dimensions of the bucket are

$$\Delta t = \frac{2\pi}{h\omega_0} \text{ (full width)} \tag{2.47}$$

$$\Delta\varepsilon = \pm\left(\frac{2EV_0}{\pi h \eta}\right)^{1/2} \tag{2.48}$$

The typical phase-space area occupied by high energy proton beams is determined by the injectors

$$\Delta\varepsilon\ \Delta\tau \sim 1\text{-}2 \text{ eV-sec} \tag{2.49}$$

For the 2020 RF system, the nominal bucket area (still neglecting the synchrotron radiation) is much larger. We have

$$\Delta\varepsilon\ \Delta\tau \sim \frac{6\sqrt{EV_0}}{h^{3/2}\omega_0\eta^{1/2}} \tag{2.50}$$

Putting in the numbers with $\Delta\tau=2\times10^{-9}$sec gives,

$$\Delta\varepsilon_{max} \sim \pm\ 150 \text{ GeV} \tag{2.51}$$

and

$$(\Delta\varepsilon\ \Delta\tau)_{RF\ bucket} \lesssim 300\ \text{eV-sec.} \tag{2.52}$$

If one puts in a bunch with the nominal, small longitudinal phase space, it will evidently not occupy the full bucket area. Its dimensions will typically be in proportion to the bucket dimensions; hence (in the absence of synchrotron radiation effects)

$$\Delta\varepsilon \sim \left(\frac{\text{Phase-space area}}{\text{Bucket area}}\right)^{1/2} \Delta\varepsilon_{max} \sim \frac{150\ \text{GeV}}{(150\text{-}300)^{1/2}} \sim 10\ \text{GeV}$$

$$\Delta\tau \sim 10^{-10}\ \text{sec.} \tag{2.53}$$

This would imply a bunch length

$$\Delta s \sim c\Delta\tau \sim 3\ \text{cm.} \tag{2.54}$$

If RF acceleration is present and $\phi_0 \neq 0$, the bucket size decreases and the bucket shape becomes similar to a fish, as shown in Fig. 6. However, the nominal order of magnitude estimates which we made will not be changed. An accurate discussion of this can be found in many places in the literature.[5]

We note that at energies less than 500 TeV, the synchrotron radiation loss becomes quite small and the RF system is suitable for acceleration of the beam from injection energy (~70 TeV??). The time Δt required for acceleration to top energy is

$$\Delta t \sim \frac{500\ \text{TeV}}{250\ \text{Hz}\times 3\ \text{GeV}} \sim 10\ \text{minutes} \tag{2.55}$$

which is reasonable.

To get an idea of the scale of this RF system, we note that in the LEP design at maximum energy the synchrotron loss per turn is ~2.4 GeV. The RF system (350 Mhz) is 1.6 km long and consumes ~100 MW. For the 2020 machine we therefore need ~3 km of RF with nominal power consumption (without considering future improvements such as superconducting RF) of ~200 MW. On the scale of this machine, these requirements are quite modest.

6. Radiation Damping

Emission of synchrotron radiation leads to damping of the phase space population of the beam. Consider first the vertical degrees of freedom. Synchrotron radiation is emitted along the direction of motion of the particle (to accuracy of order $\gamma^{-1}=(m/E)$). Thus when a photon is emitted, the transverse momentum is diminished by the same percentage as the longitudinal momentum. But only the loss in longitudinal momentum is compensated by the RF system. Hence the transverse momentum (better, phase-space area) diminishes in accordance with the rate of energy loss from synchrotron radiation.

$$\frac{1}{(\Delta p_z \Delta z)} \frac{d}{dt} (\Delta p_z \Delta z) \simeq \left(\frac{U_0}{E}\right)\left(\frac{\omega_0}{2\pi}\right) \tag{2.56}$$

or

$$(\Delta p_z \Delta z)_t = (\Delta p_z \Delta z)_0 \, e^{-t/\tau_v} \tag{2.57}$$

with the damping time τ_v given by

$$\tau_v = \frac{E}{U_0} \frac{2\pi}{\omega_0} \tag{2.58}$$

It is the time required for a particle to emit an amount of synchrotron-radiation energy equal to its own energy. For the 2020 machine, we get

$$\tau_v \sim 20 \text{ min.} \tag{2.59}$$

Notice that the scaling law is

$$\tau_v \sim \frac{R^2}{E^3} \sim \frac{1}{EB^2} \tag{2.60}$$

with B the magnetic field in the ring.

Horizontal motion is in principle more complicated because momentum dispersion and betatron oscillations are both damped, but are in fact coupled. But the complications are inconsequential, and to good approximation

$$\tau_h \simeq \tau_v \tag{2.61}$$

The momentum spread is also damped. This can be readily seen by returning to Eqn. (2.38) and keeping the damping-term (obtained by expanding the energy loss due to synchrotron radiation through first order in ε.) Since

$$U_0 \sim \frac{(E_0+\varepsilon)^4}{R} \tag{2.62}$$

we have, to good approximation*

$$\frac{\partial U_0}{\partial \varepsilon} \cong 4\,\frac{U_0}{E_0} \tag{2.63}$$

Reconstruction of the oscillator equation, keeping track of the damping term, leads for small amplitudes to

$$\frac{d^2\tau}{dt^2} = -\,\Omega_s^2\tau + \frac{4U_0}{E_0}\,\frac{\omega_0}{2\pi}\,\frac{d\tau}{dt} \tag{2.64}$$

and thus

$$\tau(t) = \tau_0\, e^{i\Omega_s t}\, e^{-t/\tau_s} \tag{2.65}$$

with

$$\tau_s = \frac{1}{2}\tau_h = \frac{2\pi}{\omega_0}\,\frac{E_0}{2U_0} \tag{2.66}$$

7. Quantum Excitation

At this stage we would infer that with time the beam phase-space would shrink to a point, with a characteristic time equal to the time required for a particle to radiate its energy into synchrotron photons. That is too good to be true and other effects must intervene. The dominant effect (for beams of sufficiently low intensity) arises from the same source, namely the quantum nature of the emitted radiation. Quantum fluctuations produce noise; the particle energy random-walks away from the mean

*Strictly speaking, R is a function of ε. But this contribution is easily shown for our big machine to be small because of the smallness of $\langle\eta(s)\rangle$.

energy, being limited only by the damping time itself. The energy fluctuation is therefore

$$\Delta E \sim \sqrt{n_\gamma}\, E_c \tag{2.67}$$

where n_γ is the number of photons emitted during a damping period and E_c (eqn. 2.28) is the typical photon energy.

$$n_\gamma \sim \sqrt{\frac{E}{E_c}} \tag{2.68}$$

or*

$$\frac{\Delta E}{E} \simeq \sqrt{\frac{E_c}{E}} \tag{2.69}$$

For the 2020 machine this means

$$\frac{\Delta E}{E} \sim \sqrt{\frac{300\text{keV}}{500\text{TeV}}} \sim 2.5\times10^{-5} \tag{2.70}$$

and a horizontal spread

$$x_\varepsilon \sim \eta\, \frac{\Delta E}{E} \sim 20\mu \tag{2.71}$$

These energy fluctuations drive horizontal betatron oscillations; x_β can neither dominate x_ε nor be negligible with respect to x_ε:

$$x_\beta \sim x_\varepsilon \tag{2.72}$$

A detailed discussion can be found in Sands.[6]

So far the vertical motion is not affected by quantum excitation. While there is some vertical spread caused by the angular distribution of emitted photons, this is negligible in comparison to vertical spread induced by higher order effects (skew quadrupoles, nonlinear elements such as sextupole and octupole fields; noise, etc.) These are not easy (certainly not here) to quantify. Empirically one finds in e^+e^- machines beam heights ~1–10% of the beam width

$$\Delta z \sim (.01-.1)\Delta x \tag{2.73}$$

*This implies that $\Delta E/E \sim E/\sqrt{\rho}$. For electron machines, design considerations force $\rho \sim E^2$ in order to minimize the sum of RF costs ($\alpha\ E^4/\rho$) and ring costs ($\alpha\ \rho$). Hence $\Delta E/E$ is roughly machine-independent.

If true for the 2020 machine, this would imply

$$\langle \Delta z \rangle \lesssim 2\mu \tag{2.74}$$

More important than the actual size is the distribution in z or x. The noisy nature of the quantum-fluctuation mechanism suggests a gaussian distribution. However, this driving mechanism, when coupled with the effects of nonlinear forces (beam-beam interaction, resonances, etc.), turns out to produce much longer (roughly exponential) tails. Formulation of diffusion-equations for the phase-space population is necessary to treat this question. Of course, the magnitude of the tail of the distribution at the machine aperture determines the rate of beam loss.

In proton machines at present energies, where synchrotron radiation is negligible, the tail of the transverse density distribution is much sharper. The dynamics which determines the nature of this distribution is obscure and has to do with nonlinearities in the optical properties of the lattice, the beam-beam interaction, the number and strength of nearby resonances, and sources of noise (power-supply ripple, RF noise, and gas scattering).

8. Collective (Single-Beam) Instabilities

There exist a large class of instabilities which occur because of the interaction of a single beam with its environment. The electromagnetic field of the beam induces currents in the walls of the vacuum chamber, which in turn create fields which drive the beam. If the beam intensity is high enough and the phase relation of the response to the source is "correct," there may be positive feedback and creation of instability.

There are both transverse and longitudinal instabilities. Some instabilities depend on coupling to resonant structures of high Q (eg RF cavities). Others are present even in a non-resonant environment. We shall not recite here the catalogue of instabilities. But the most serious ones are those with high frequency, where a single bunch executes complex internal motion of nontrivial "multipolarity," rather than rigid motion.

Rigid motion of an entire bunch may be monitored, and there is the opportunity to cure the instability via feedback. The high-frequency "microwave" instability must be cured by other means. The most serious such instability for the 2020 machine appears to be longitudinal and we briefly describe this one, in order to give some idea of how these are handled.

Consider first of all a <u>coasting</u> beam which has a small periodic density modulation as function of longitudinal coordinate s. (We ignore the transverse degrees of freedom.) The image charge and wall current will likewise be modulated, and exert a force back on the beam which is periodic with the same frequency. We consider* this frequency ω to be a multiple n of the revolution frequency ω_0. Then the beam finds itself in a RF potential $V(\omega)$ which may, if the phase relations are appropriate, tend to bunch the beam, thereby increasing the image currents, which in turn leads to increased bunching and ultimate instability. The induced RF voltage $V(\omega)$ will be linearly related to the perturbing current $i(\omega)$ (due to the linearity of Maxwell's equations)

$$V(\omega) = i(\omega) Z_{||}(\omega) \tag{2.75}$$

This relation defines the (complex) impedance, a quantity which can be calculated by solving Maxwell's equations for the electromagnetic fields produced in the vacuum chamber by the perturbed circulating beam.[8]

For instability to ensue, $V(\omega)$ must be large enough to capture the beam, i.e. to bunch the beam and contain the beam phase-space within the (self-consistently induced) RF buckets. The bucket height is given by Eqn (2.48), with the harmonic number given by n:

$$(\Delta E)^2 \sim \frac{EV}{\eta n} = \frac{E}{\eta}\frac{Z_{||}}{n}\, i \tag{2.76}$$

Thus large momentum spread and/or low currents are necessary to avoid the instability. (This is the Keil-Schnell criterion[9]):

$$\frac{Z_{||}}{n} \cdot i \leq \eta E \left(\frac{\Delta E}{E}\right)^2 \tag{2.77}$$

For the "microwave" instability, the important wavelengths are smaller than the bunch length (Δs). The impedance on the other hand decreases as the frequency exceeds cd^{-1}, where d is the beam-pipe diameter. Then in evaluating Eqn (2.77), in this case, we must use the <u>peak</u>, or instantaneous current in the bunch, inasmuch as the instability is locally generated and would be

*If this is not the case the "induced" RF system can be thought of as rotating around the machine at the difference frequency.

equally important were the ring filled with bunches. That is, even though the Keil-Schnell criterion was derived for coasting beams, it can be applied to the bunched beam case.[10]

We shall not estimate the impedance $Z_{||}/n$ at all. It gets many contributions from miscellaneous elements around the ring (vacuum bellows, position monitors, RF cavities, etc.), especially those with discontinuities in radius or shape, and is reputed to be difficult to compute reliably. In any case $Z_{||}$ is roughly proportional to circumference. But for a given frequency ω, the harmonic number n is also proportional to circumference. Thus $Z_{||}/n$ is an intensive quantity, roughly independent of energy. Empirically, for present machines

$$\frac{Z_{||}}{n} \gtrsim 1\text{–}10 \text{ ohms} \tag{2.78}$$

at the relevant wavelength of order a few cm.

We may now attempt some numbers. We choose $Z_{||}/n \sim 3$ ohms, and take two cases. One is that of "short bunches," where the synchrotron damping has reduced the momentum spread and bunch length. This will, as we shall see, severely limit the number of particles per bucket. The opposite extreme is to fill the bucket (more or less; we take ~25%) thereby maximizing ΔE and Δs, and minimizing the peak current. The parameters we choose are

	Short Bunch	Long Bunch	
Bunch length Δs	3 cm.	30 cm.	
Energy spread ΔE	±10 GeV	±75 GeV	(2.79)

Then the number N of particles per bunch is limited by the Keil-Schnell criterion as follows.

$$N \lesssim \begin{cases} 3\times10^{8} & \text{short bunch} \\ 2\times10^{11} & \text{long bunch} \end{cases} \tag{2.80}$$

For the "natural" short bunch, this is quite a severe limitation; intensities of 3×10^{10} to 10^{11}/bunch are the norm in present machines. To see what is optimal, however, one must look with care at the questions of luminosity and of beam-beam tune shift.

9. Luminosity

Let us put one bunch of p's and one of $\bar{p}$'s into the machine. The luminosity $\mathscr{L}$ per crossing (for head-on collisions and ignoring density variations across the bunch) is

$$\mathcal{L} \simeq \frac{N^2}{A} \tag{2.81}$$

where A is the area of the bunches and N the number of particles per bunch (Luminosity x cross-section = no. of events). We get, for the limiting cases of short and long bunch we considered in the previous section, and using just the nominal area of the beams in the machine,

	Short Bunch	Long Bunch	
N	3×10^{8}	2×10^{11}	
Area	$\sim2\mu\times20\mu$	$70\mu\times70\mu$	
$\mathcal{L}$ (per crossing)	2×10^{23} cm^{-2}	8×10^{26} cm^{-2}	(2.82)

In the case of the long bunch, we have assumed a size as determined by the betatron motion. Typically the dispersion function $\eta(s)$ is designed to vanish at the collision point, so that the horizontal size at the collision region is controlled only by the betatron phase space.

The case of the "long bunch" would lead to a quite respectable luminosity already, when one considers that the revolution frequency is 250 Hz, that the beam can be focussed more strongly at the collision point than at typical points around the ring, and that we can contemplate having a large number of bunches stored in the ring. However, there is yet another limitation to consider. This is imposed by the beam-beam interaction. Before any serious optimization of luminosity can be attempted, the beam-beam limit must be taken into account.

10. Beam-beam limit

The proton beam, through which the antiprotons necessarily pass, is a (nonlinear) focussing element for the antiprotons (and vice versa). Let us estimate the focussing strength. To simplify the discussion, approximate the proton beam by a uniform slab of charge of half-width Δx and half-height $\Delta z \ll \Delta x$. Consider only the vertical force, which for this "slab" geometry is dominant. Then the vertical impulse received by an antiproton with impact parameter z is easily worked out (most easily in the rest frame of the proton bunch).

$$\Delta p_z = e\int ds\ E_T\left(\frac{z}{\Delta z}\right) = \frac{Ne^2 z}{2\Delta x\Delta z} \qquad (z \leq \Delta z) \tag{2.83}$$

We may compare this kick to that given by a lattice quadrupole. This is (cf. Eqn. (2.8)

$$(\Delta p_z)_{quad} \sim eG\ell z \sim \frac{p}{L} z \tag{2.84}$$

The (Δp_z) from this quad changes the betatron tune ν_z by an amount $\Delta\nu$ which is O(1). Thus we get*

$$(\Delta\nu)_{Beam-beam} \simeq \frac{(\Delta p_z)_{Beam-beam}}{(\Delta\ p_z)_{quad}} \sim \frac{e^2 N}{2\Delta x \Delta z} \cdot \frac{L}{p} \tag{2.85}$$

The (linear) tune shift can be compensated by retuning quadrupoles. However, some of the beam (and after many turns, almost all of the particles) have impact parameters $z>\Delta z$ and suffer a smaller $\Delta\nu$ than the core. Thus $\Delta\nu$ is better regarded as a tune spread. As we discuss later, in order to maintain stability the tune of the machine cannot be an integer or integer plus a vulgar fraction p/q (p,q small integers). In practice the tune must be controlled to a few percent of an integer. For e^+e^- machines, the empirical (and to some extent theoretical)[11] limit on $\Delta\nu$ is $\lesssim .03$ for PEP/PETRA/CESR and $\lesssim .06$ for SPEAR/DORIS.[11]

For proton rings at present-day energies it is believed that the maximum allowed $\Delta\nu$ probably is smaller than that, owing to the lack of synchrotron-radiation damping as a stabilizing** influence. Recent experience at the CERN $p\bar{p}$ collider indicate stable operation at $\Delta\nu \sim 2\text{-}3\times10^{-3}$, in accordance with theoretical estimates.

*We have assumed the focussing strength at the collision point is typical of that around the ring. This is typically not the case. Very strong local focussing is used to increase the luminosity. If the "focal length" is smaller, then L should be replaced by the local focal length (more precisely the β-function at the collision point, to be discussed in the next section). However, then the area $A=\Delta z\Delta x$ should be replaced by the (smaller) local value as well. It turns out that A is also proportional to L, so that the beam-beam tune shift is independent of the local focussing strength.

**After a damping time the electron beam forgets its past. Protons at present energies, like elephants, never forget. But for electrons the radiation excitation introduces more noise into the phase-space, a destabilizing influence.

Our 2020 machine is an intermediate case; we assume $\Delta\nu \lesssim .01$ is the limit (good to a factor 3). Putting in some rough numbers then gives, for single bunches and our previous parameters,

$$\Delta\nu_{\text{beam-beam}} \overset{?}{\sim} \begin{matrix} .06 & \text{"short" beam} \\ 0.3 & \text{"long" beam} \end{matrix} \qquad (2.86)$$

This is unacceptable, and we must optimize the luminosity taking simultaneously into account the synchrotron damping, the limit on single-beam current from the microwave instability, and the limit from beam-beam tune shift.

We note here that the beam-beam limit, Eqn. (2.83), implies a maximum value for the transverse current density. To increase luminosity it is advantageous to make the beam <u>bigger.</u> In particular, dividing Eqn. (2.80) by (2.83), we get

$$\mathcal{L} \sim \frac{N\Delta\nu}{2\pi\alpha} \cdot \frac{p}{L} \qquad \text{(per crossing)} \qquad (2.87)$$

Thus for fixed $\Delta\nu$ and p, our options are

1) Increase N, at the same time somehow <u>increasing</u> the area A.

2) Decrease L, i.e. make the focussing at the collision point as strong as possible.

We shall not pursue these issues further here, but will wait until we have built up more formalism. Suffice it to say that we do not yet have <u>any</u> reliable luminosity estimate.

III. OPTICS

1. <u>Vertical Motion; Hill's Equation</u>

In this section we shall discuss in more detail how one describes the optics of the machine. We begin as before with vertical motion, and write down the basic equations:

$$z' \equiv \frac{dz}{ds} \qquad (3.1)$$

$$\frac{dz'}{ds} = -\,k(s)z \qquad (3.2)$$

Here

$$z' \equiv \frac{p_z}{p} = \Theta_z \tag{3.3}$$

the derivative of the vertical coordinate is used as a momentum variable rather than p_z. Thus phase space is conventionally taken to be z-z' space.

The focussing function $k(s)$ is (to first approximation), for an ideal alternating gradient lattice, nonvanishing only within quadrupole magnets, where

$$k(s) \equiv \pm \frac{eG}{p} = \pm \frac{G}{B\rho} \tag{3.4}$$

The two first-order equations combine to produce an oscillator-like equation.

$$z'' + k(s)z = 0 \tag{3.5}$$

This is known as Hill's equation. The focussing function is periodic, $k(s) = k(s+C)$, with C the orbit circumference. But general solutions, of course, need <u>not</u> be periodic.

Were k a constant, we would have oscillatory motion.

$$z \sim z_0 \sin\left(\frac{s}{\beta} + \phi_0\right) \tag{3.6}$$

$$z' \sim \frac{z_0}{\beta} \cos\left(\frac{s}{\beta} + \phi_0\right) \tag{3.7}$$

with

$$\beta = \frac{1}{\sqrt{k}} \tag{3.8}$$

a constant. The set of all orbits of constant amplitude would form in z,z',s phase space a tube (or torus if z is closed back upon itself: $z+C=z$), with individual orbits following helical paths around the tube, as shown in Fig. 7.

<u>Provided stable solutions exist</u>, the general solution to Hill's equation has a similar form. It is conventionally written

$$z = \sqrt{\beta(s)\varepsilon}\,\sin\phi(s) \tag{3.9}$$

where the amplitude function $\beta(s)$ is periodic and depends only upon the lattice, i.e. the focussing function $k(s)$. The constant ε, called the Courant invariant, determines the normalization of the amplitude. The phase function $\phi(s)$ is determined by $\beta(s)$ as follows

$$\phi(s) = \int_{s_0}^{s} \frac{ds}{\beta(s)} \tag{3.10}$$

This latter relation can be obtained by substituting the "solution", Eqn (3.9) into Hill's equation, and demanding the coefficient of cos ϕ vanish.* The vanishing of the coefficient of sin ϕ then produces a nonlinear second order differential equation for β that we shall not bother to write down. There are other convenient ways of obtaining the β-function, which we shall describe later on.

The amplitude function $\beta(s)$ is a most important function; it determines the (linear) optical properties of the lattice, and essential properties of the vertical motion. In particular the tune ν (the number of betatron oscillations per revolution) now has a precise definition

$$\nu = \frac{1}{2\pi} \oint \frac{ds}{\beta(s)} \tag{3.11}$$

2. Linear Maps

We may obtain more insight into the motion and determine $\beta(s)$ as well by going back to the Hamiltonian form of two first-order equations for z and z'. In this form the content of the Liouville theorem is more directly seen.

First order linear equations can (like the Schrodinger equation) be formally integrated. Define

$$\xi(s) = \begin{pmatrix} z(s) \\ z'(s) \end{pmatrix} \tag{3.12}$$

and relate $\xi(s+ds)$ to $\xi(s)$. From Eqns (3.1) and (3.2)

$$\xi(s+ds) = \left[\begin{pmatrix} 1 & 0 \\ 0 & 1 \end{pmatrix} + \begin{pmatrix} 0 & 1 \\ k(s) & 0 \end{pmatrix} ds\right] \xi(s) \equiv (1+Tds)\xi(s) \tag{3.13}$$

*The constant of integration one gets is set to zero. This cleans up the equation for β.

and hence $\xi(s')$ can be obtained from $\xi(s)$ by multiplying by a product of matrices each of which depend only on the lattice. For sufficiently small Δs we have, schematically

$$\xi(s') = M(s',s)\xi(s) = [\prod_{\Delta s} (1+T\Delta s)]\xi(s) \tag{3.14}$$

[A veteran particle theorist will write

$$M(s',s) = P \exp \int_s^{s'} ds''T(s'') \tag{3.15}$$

where P is the path ordering operator.]

The matrix $M(s',s)$ is known as the <u>transport matrix.</u> Because a lattice is composed of a sequence of basic elements and because transport matrices satisfy the group property

$$M(s'',s')M(s',s) = M(s'',s) \tag{3.16}$$

we need only know the matrices for the basic elements. For example

$$M = \begin{pmatrix} 1 & 0 \\ -\frac{1}{f} & 1 \end{pmatrix} \quad \begin{array}{l} \text{Thin focussing quadrupole*} \\ \\ \text{(For defocussing, } f \to -f) \end{array}$$

$$M = \begin{pmatrix} 1 & L \\ 0 & 1 \end{pmatrix} \quad \begin{array}{l} \text{Bending magnet or straight} \\ \text{section of length L.} \end{array} \tag{3.17}$$

Here the focal length is

$$\frac{1}{f} = \frac{eG\ell}{p} = \frac{G\ell}{B\rho} \tag{3.18}$$

Then ξ can be propagated around the ring by multiplying these 2×2 matrices together. Note that the determinant of the matrix for a basic element is unity; hence so also is a product of them

$$\det M(s',s) = 1 \tag{3.19}$$

[This is directly related to the Liouville theorem.]

*For accuracy, one must go beyond the thin lens approximation. For our purposes this is hardly necessary. The reader is invited to work out the correction using the basic elements given here.

Now consider the matrix for a complete circuit around the ring. After N revolutions the coordinate is

$$\xi^{(N)} = M^N \xi^{(0)} \tag{3.20}$$

If we diagonalize M

$$SMS^{-1} = \begin{pmatrix} \lambda_1 & 0 \\ 0 & \lambda_2 \end{pmatrix} \tag{3.21}$$

we must have

$$\lambda_1 \lambda_2 = 1 \tag{3.22}$$

and for stability

$$\begin{aligned} \lambda_1 &= e^{i\phi} \\ \lambda_2 &= e^{-i\phi} \end{aligned} \tag{3.23}$$

(Otherwise $\xi^N \sim \lambda^N{}_{max}$ grows exponentially with N)

$$\mathrm{Tr}\ M(s+C,s) = \mathrm{Tr}\ SMS^{-1} = 2\cos\phi < 2 \tag{3.24}$$

is sufficient to ensure stability. It takes little imagination to guess that ϕ is essentially the tune

$$\phi = 2\pi\nu \tag{3.25}$$

[We leave the demonstration to the reader.] We may also obtain $\beta(s)$ from the transport matrix M(s+C,s). Recall, from Eqn. (3.9), along with one differentiation,

$$\xi = \begin{pmatrix} z(s) \\ z'(s) \end{pmatrix} = \begin{pmatrix} \sqrt{\beta(s)\varepsilon}\,\sin\phi(s) \\ \sqrt{\dfrac{\varepsilon}{\beta(s)}}\cos\phi(s) + \dfrac{\beta'}{2}\sqrt{\dfrac{\varepsilon}{\beta(s)}}\sin\phi\,(s) \end{pmatrix} \tag{3.26}$$

Now choose the initial phase such that $\phi(s)=0$ and initial amplitude $\varepsilon=\beta$. Then

$$\xi(s) = \begin{pmatrix} 0 \\ 1 \end{pmatrix} \tag{3.27}$$

After one revolution

$$\xi(s+C) = \begin{pmatrix} \beta(s)\sin 2\pi\nu \\ \cos 2\pi\nu + \frac{\beta'}{2}\sin 2\pi\nu \end{pmatrix} \tag{3.28}$$

But from the definition of the transport matrix and Eqn. (3.27)

$$\xi(s+C) = \begin{pmatrix} M_{12} \\ M_{22} \end{pmatrix} \tag{3.29}$$

and thus the upper right-hand element of M(s+C,s) determines directly β(s). This clearly provides a convenient numerical procedure. Using the constraints on Tr M and det M, the general form of M(s+C,s) is

$$M = \cos 2\pi\nu + J\sin 2\pi\nu = e^{2\pi\nu J} \tag{3.30}$$

with

$$J = \begin{pmatrix} -\frac{\beta'}{2} & \beta \\ -\frac{1}{\beta}(1+\frac{\beta'^2}{4}) & \frac{\beta'}{2} \end{pmatrix} \tag{3.31}$$

Note that $J^2=-1$.

We repeat:

To obtain the tune ν and the β-function β(s):
Compute the transport matrix for a complete revolution. Then
$\mathrm{Tr}\, M(s+C,s) = 2\cos 2\pi\nu$
$M_{12} = \beta(s)\sin 2\pi\nu$ (3.32)

The reader should not delude himself into thinking that this sketch provides a strict derivation of the results we have presented. However, the raw material for providing the missing links <u>has</u> been given.

3. Nature of the Motion

We have already described the nature of the motion in the case of a constant focussing function k(s). For the general case of stable motion there is in z, z', s space again an "invariant torus" on which all orbits with a given value of Courant-invariant ε lie; these orbits again spiral around the torus. At any given s, the cross-section of the torus is an ellipse, as can be seen from Eqn (3.26) and $\cos^2 + \sin^2 = 1$

$$\varepsilon = \frac{z^2}{\beta(s)} + \beta(s)\left(z' - \frac{\beta'}{2\beta} z\right)^2 \tag{3.33}$$

The area of the ellipse is independent of s (Liouville again!) and is $\pi\varepsilon$. At extrema of $\beta(s)$ we have an erect ellipse; in between extrema it is skew (cf. Fig. 8). Note the β-function does not describe the orbit of a given particle but rather the envelope of many particle orbits.

For a beam, i.e. a phase space population, the typical value of the phase space area of the particles in the beam is called the emittance of the beam (careful! sometimes what is quoted is 1σ; other times 2σ):

$$\text{emittance} = \langle\varepsilon\rangle = \pi\sqrt{\langle z^2\rangle\langle z'^2\rangle} \tag{3.34}$$

The maximum value of emittance which survives in the machine is called admittance or aperture.

4. FODO Lattice

We now compute $\beta(s)$ for a FODO lattice. This is, as already described in the previous section, a regular sequence of focussing and defocussing quads separated by bending magnets. We first compute the transfer matrix for a cell (the basic element of the lattice consisting of one F quad, one D quad, and the intervening magnets). We again assume the quads are separated by distance L and start the transfer matrix from the center of an F quad, where by symmetry we expect an extremum of the β-function. Then first calculate [cf. Eqn. (3.17)]

$$\sqrt{F}\, O\, \sqrt{D} \equiv \begin{pmatrix} 1 & 0 \\ -\frac{1}{2f} & 1 \end{pmatrix} \begin{pmatrix} 1 & L \\ 0 & 1 \end{pmatrix} \begin{pmatrix} 1 & 0 \\ \frac{1}{2f} & 1 \end{pmatrix}$$

$$= \begin{pmatrix} 1 + \frac{L}{2f} & L \\ -\frac{L}{4f^2} & 1 - \frac{L}{2f} \end{pmatrix} \tag{3.35}$$

Next calculate $\sqrt{D}O\sqrt{F}$ which is easy; just change $f \to -f$. Then multiply the two together to get

$$\sqrt{F}\,O\,D\,O\,\sqrt{F} = \begin{pmatrix} 1 - \frac{L^2}{2f^2} & 2L(1 + \frac{L}{2f}) \\ \text{etc.} & 1 - \frac{L^2}{2f^2} \end{pmatrix} \tag{3.36}$$

By symmetry the β-function is periodic over a cell as well as over the entire machine. Therefore we can define a phase advance per cell μ such that

$$2\pi\nu = \mu\, n_{cells} \tag{3.37}$$

and use the transport matrix for a cell rather than for the whole machine to obtain the β-function β_{max} at the focussing quad. According to our recipe

$$\cos\mu = 1 - \frac{L^2}{2f^2}$$

$$\beta_{max}\sin\mu = 2L(1 + \frac{L}{2f}) \tag{3.38}$$

or

$$\beta_{max} = 2f\sqrt{\frac{1 + \frac{L}{2f}}{1 - \frac{L}{2f}}} \tag{3.39}$$

Note that, as expected, $\beta' = 0$. Also by replacing $F \to D$ we get β_{min} and

$$\frac{\beta_{max}}{\beta_{min}} = \frac{1 + \frac{L}{2f}}{1 - \frac{L}{2f}} = \frac{1 + \sin\frac{\mu}{2}}{1 - \sin\frac{\mu}{2}} \tag{3.40}$$

We may observe that for stability we must have

$$\frac{L^2}{2f^2} < 2 \tag{3.41}$$

or

$$f > \frac{L}{2} \tag{3.42}$$

That is, we must not overfocus. In practice a phase advance per cell of $\sim 90^0$ (sometimes a little less)

$$\mu \lesssim \frac{\pi}{2}$$

$$f \lesssim \frac{L}{\sqrt{2}} \tag{3.43}$$

is chosen. We shall take $\mu = \pi/2$ for definiteness. Note also that, because

$$\frac{1}{f} = \frac{eG\ell}{p} \tag{3.44}$$

the above condition is

$$\frac{eG\ell L}{p} = \frac{G\ell L}{B\rho} = \sqrt{2} \tag{3.45}$$

which is essentially what we saw in the previous section (cf.Eqn.(2.8)). Note also that

$$\langle\beta\rangle \sim 2f \sim \sqrt{2}\, L \tag{3.46}$$

so that the fuzzy parameter L used in the previous section should be replaced by the basic optical parameter $\beta(s)$, which measures the local betatron wavelength according to the relation, Eqn.(3.10):

$$\Delta\phi = \frac{\Delta s}{\beta(s)} \tag{3.47}$$

The β-function in between F and D magnets can be obtained by the same technique but by employing a different starting point. This is left as an exercise.

5. Horizontal motion and dispersion

The betatron motion in the horizontal plane, as mentioned in the previous section, is almost the same as for the vertical plane. Inclusion of the curvature correction in Hill's equation gives

$$\frac{d^2x}{ds^2} + k(s)x + \frac{x}{\rho^2} = 0 \tag{3.48}$$

i.e. bending magnets produce a little focussing. (This should be put into the matrix O for a bending magnet.)

The dispersion function $\eta(s)$ describing the closed orbit deviation x_ε for off-momentum particles

$$x_\varepsilon = \eta(s)\frac{\Delta p}{p} \equiv \eta(s)\sigma_\eta \tag{3.49}$$

may now be calculated. To first order, contributions to the dispersion function, which evidently is periodic over a cell, come only from bending magnets (which are analogous to prisms). A magnet of length L contributes deviations δx and $\delta x'$ given by (cf. Fig.)

$$\begin{pmatrix} \delta x \\ \\ \delta x' \end{pmatrix} = \begin{pmatrix} \frac{L^2}{2\rho^2} \\ \\ \frac{L}{\rho^2} \end{pmatrix} \delta\rho = \begin{pmatrix} \frac{L^2}{2\rho} \\ \\ \frac{L}{\rho} \end{pmatrix} \sigma_\eta \equiv \Delta \tag{3.50}$$

Let

$$\xi(s) = \begin{pmatrix} \eta(s) \\ \\ \eta'(s) \end{pmatrix} \sigma_\eta \tag{3.51}$$

be the orbit deviation. The change in orbit deviation over a cell is then expressed by

$$\xi(s+2L) = M(s+2L,s)\xi(s) + \sqrt{F}\Delta + \sqrt{F}OD\Delta \tag{3.52}$$

where the last two inhomogeneous terms are contributed by the magnets in the cell, and the first term propagates the orbit error through the cell. By symmetry

$$\xi(s+2L) = \xi(s) \equiv \xi_{max} \tag{3.53}$$

and we get

$$\xi_{max} = \frac{1}{1-M}\sqrt{F}(1+OD)\Delta \tag{3.54}$$

This determines the maximum value of $\eta(s)$. Evaluation of the right hand side is done via the following steps:

1. Explicity work out the numerator.

2. Determine eigenvectors of M.

3. Expand the numerator in terms of these eigenvectors.

4. Evaluate ξ_{max}.

One finds

$$\eta_{max} = \frac{L^2}{\rho \sin^2 \frac{\mu}{2}} \left(1 + \frac{1}{2}\sin\frac{\mu}{2}\right) \qquad (3.55)$$

with η_{min} obtained, as usual by changing +1/2 to -1/2 in the numerator. Putting in numbers for $\mu=\pi/2$ gives

$$\eta_{max} = 2.7\,\frac{L^2}{\rho} \qquad \eta_{min} = 1.3\,\frac{L^2}{\rho} \qquad (3.56)$$

From Eqn. (3.45) (for $\mu=\pi/2$)

$$\sqrt{2} = \frac{eG\ell L}{p} = \frac{G\ell L}{B\rho} = \frac{G}{B}\cdot\frac{\ell}{L}\cdot\frac{L^2}{\rho} \qquad (3.57)$$

Hence, for 90° phase advance/cell

$$\eta_{max} \equiv 4\left(\frac{B}{G}\cdot\frac{L}{\ell}\right) \qquad (3.58)$$

which is, as advertised, independent of energy, and of order meters.

A more systematic way of treating dispersion[12] is to enlarge the transport matrix to a 3x3 matrix which acts upon x, x', and σ_η.

6. Chromaticity

Not only does the closed orbit change for off-momentum particles but also the focal properties of the lattice – in particular the tune ν. The optical analogue is chromatic aberration. Thus the chromaticity ξ is defined as the percent change in tune per percent change in momentum

$$\frac{\delta\nu}{\nu} = \xi\frac{\delta p}{p} = \xi\sigma_\eta \qquad (3.59)$$

The natural chromaticity, which is the contribution to ξ of the normal lattice, can be computed directly. From Eqn. (3.38).

$$\cos\mu = 1 - \frac{L^2}{2f^2} \qquad (3.60)$$

and

$$\frac{\delta f}{f} = -\frac{\delta p}{p} \tag{3.61}$$

one finds easily that

$$\frac{\delta\nu}{\nu} = \frac{\delta\mu}{\mu} = -\frac{2}{\mu} \tan\frac{\mu}{2}\frac{\delta p}{p} \tag{3.62}$$

For 90° phase advance, this gives

$$\xi = -1.3 \tag{3.63}$$

This is too large and, as it turns out, also of the wrong sign. Single-beam instabilities are sensitive to chromaticity, and stability requires a positive value. The chromaticity is adjusted by adding sextupole magnets around the ring. Evidently the sextupole strength (per cell) needed to do this scales with the quadrupole strength, independent of energy.

IV. ERRORS AND NONLINEAR RESONANCES

With such a big machine, we might expect it to be impossible to align. We briefly investigate here the effect of errors and nonlinearities.

1. Closed orbit error.

Suppose one magnet at position s_0 provides the wrong bending field by an amount ΔB. The normal bend angle $\Delta\theta$ in the magnet is

$$\Delta\theta = \frac{eB\Delta s}{p} = \frac{\Delta s}{\rho} \tag{4.1}$$

Then the angle change $\delta x'$ caused by the error is

$$\delta x' = \frac{\Delta B}{B}\Delta\theta \sim \frac{\Delta B}{B}\frac{\Delta s}{\rho} \tag{4.2}$$

Therefore the perturbed closed orbit is just a betatron oscillation which has a kink in slope of magnitude $\delta x'$ located at s_0. We need therefore to simply locate a phase point $\xi(s_0)$ such that $x(s_0+C)=x(s_0)$ and $x'(s_0+C)=\delta x'+x'(s_0)$. Write

$$x(s_0)=\sqrt{\beta\varepsilon}\cos\phi_0 \tag{4.3}$$

Then

$$x(s_0+C) = \sqrt{\beta\varepsilon}\cos(\phi_0+2\pi\nu) \tag{4.4}$$

implying $\phi_0=-\pi\nu$. We now calculate $\delta x'$:

$$x'(s_0) = \sqrt{\frac{\epsilon}{\beta}} \sin \phi_0 + \frac{\beta'}{2\beta} x(s_0) \tag{4.5}$$

and

$$x'(s_0+C) = \sqrt{\frac{\epsilon}{\beta}} \sin(\phi_0+2\pi\nu) + \frac{\beta'}{2\beta} x(s_0+C) \tag{4.6}$$

Subtraction gives us the amplitude $\sqrt{\epsilon\beta}$

$$\delta x' = x'(s_0+C) - x'(s_0) = 2\sqrt{\frac{\epsilon}{\beta}} \sin\pi\nu = \frac{\Delta B}{B\rho} \Delta s \tag{4.7}$$

and thus the solution for x (Green's function!) is

$$x(s) = \frac{\sqrt{\beta(s)\beta(s_0)}}{2 \sin \pi\nu} \left(\frac{\Delta B}{B}\right)_{s_0} \frac{\Delta s}{\rho} \cos\left(\pi\nu - \int_{s_0}^{s} \frac{ds'}{\beta(s')}\right) \tag{4.8}$$

Note that (1) the amplitude is largest if the field error is located in a region of large β, and that (2) the amplitude blows up if ν is an integer. This is the simplest kind of resonance. If on each revolution the betatron phase at s_0 is the same, the error kick will always increase the amplitude in the same way; one has just a resonantly driven oscillator.

The total contribution to the closed orbit is obtained, via superposition, by adding the contributions of the individual magnet errors. If they are random, then the rms error is

$$\langle x^2\rangle_{rms} = \frac{\beta(s)\bar{\beta}}{8 \sin^2 \pi\nu} \left\langle \left(\frac{\Delta B}{B}\right)^2 \right\rangle_{rms} \frac{\ell^2_{magnet}}{\rho^2} N_{magnet} \tag{4.9}$$

The scaling law is

$$\Delta x \sim \frac{\beta}{\rho} \cdot \left(\frac{\Delta B}{B}\right) \cdot \ell_{magnet} \cdot \sqrt{N_{magnet}} \sim \sqrt{\frac{N_{magnet}}{\nu}} \tag{4.10}$$

For fixed magnet type and magnet quality, and for $\nu \sim \sqrt{E}$, we find Δx is independent of energy. Choosing $\ell_{mag} \sim 7m$, $N \sim 1.4\times10^5$, $\nu \sim 400$, and $\Delta B/B \sim 10^{-3}$, we get $\langle\Delta x\rangle \sim$ 5mm. Correction elements are a necessity, but the problem (on paper) does not worsen with energy.

Not all errors need be random. If fourier components (in longitudinal coordinates) of the error field peak near the betatron wavelength, one can get enhancements. This is in fact one way of correcting closed orbit errors; one analyzes the Fourier spectrum of the particle orbit deviations, and applies correction (dipole) fields having the dominant Fourier component.[13]

2. Tune Shifts

Suppose a quadrupole at s_0 has the wrong field. Then the tune will be modified. To estimate this, we look at the modification to the transport matrix

$$M(s_0+C,s_0)\rightarrow\begin{pmatrix}1 & 0\\ \ell_{quad}\ \delta k & 1\end{pmatrix}M(s_0+C,s_0) \tag{4.11}$$

We need only recalculate the trace

$$\begin{aligned}\mathrm{Tr}M &\rightarrow \mathrm{Tr}M + \ell_{quad}\ \delta k\cdot M_{12}\\ &= 2\cos 2\pi\nu + \beta(s_0)\ \ell_{quad}\ \delta k\cdot\sin 2\pi\nu\end{aligned} \tag{4.12}$$

and thus

$$\begin{aligned}\Delta\nu &= \frac{\ell_{quad}}{4\pi}\beta(s_0)\delta k\\ &= \frac{1}{4\pi}\beta(s_0)\left(\frac{\Delta G}{G}\right)\cdot\frac{1}{f}\cdot\frac{\ell_{quad}}{\ell}\end{aligned} \tag{4.13}$$

The last factor takes into account the fact that for the 2020 machine (unlike present machines) what we call a focussing element F consists of a sequence of quadrupole magnets, not an individual magnet. Again, assuming random errors and averaging around the ring gives

$$\langle\Delta\nu\rangle\sim\frac{1}{4\pi}\sqrt{\frac{\beta_{max}^2+\beta_{min}^2}{2}}\ \frac{\Delta G}{G}\ \frac{\sqrt{N_{quad}}}{f}\left(\frac{\ell_{quad}}{\ell}\right) \tag{4.14}$$

Since

$$\frac{1}{f\ell}=\frac{eG}{p}=\frac{G}{B\rho} \tag{4.15}$$

we have

$$\langle\Delta\nu\rangle \sim \frac{\beta\sqrt{N}_{quad}}{\rho} \cdot \left(\frac{\Delta G}{G}\right) \cdot \frac{G}{B} \cdot \ell_{quad} \tag{4.16}$$

Again, with

$$\begin{aligned} \beta &\sim \sqrt{E} \\ \rho &\sim E \\ \sqrt{N_{quad}} &\sim \sqrt{E} \end{aligned} \tag{4.17}$$

we find a tune-shift independent of energy. Putting in numbers for the 2020 machine gives

$$\langle\Delta\nu\rangle \sim 3\langle\frac{\Delta G}{G}\rangle \tag{4.18}$$

3. Miscellaneous Errors

Other such errors can be treated similarly. A short compendium can be found in a contribution by King[14] for ICFA studies of a 20 TeV machine. They include

1. Vertical plane misalignments of dipoles.
2. Quadrupole position errors.
3. Quadrupole tilts.
4. Stray magnetic fields at injection.
5. Gradient errors in dipole magnets.

Examination of the formulae again shows that none of them scale with energy in such a way that the problems worsen at higher energy. Typically the number of sources scale linearly with energy, giving a net deviation growing as $\sqrt{N} \sim \sqrt{E}$. The betatron wavelength also scales as $\sqrt{E}$, and magnetic rigidity (a good word!) as E. The net deviation then scales as $(\sqrt{E})^2/E \sim 1$.

4. Tune Shift from Machine Nonlinearities

The magnetic fields in the lattice are not ideal. Higher order nonlinear terms are present and must be kept under control. To begin, write, for corrections from dipole magnets,

$$\Delta B_x = B_0(1 + \sum_n b_n x^n) \tag{4.19}$$

There are also cross terms in x and z (which are typically more important!), but we come back to those later. The modification to Hill's equation is

$$\frac{d^2x}{ds^2} + k(s)x = \frac{\Delta B(s)}{B\rho} = \frac{1}{\rho}\sum_n b_n(s)x^n \tag{4.20}$$

We have a change in focussing strength

$$\Delta k \sim \frac{-1}{\rho}\sum_n b_n x^{n-1} \tag{4.21}$$

which is, as one could have guessed, most important for large amplitudes. To estimate the change in tune, we may borrow Eqn. (4.13):

$$\Delta\nu = \frac{ds}{4\pi}\,\beta(s)\Delta k \tag{4.22}$$

and obtain

$$\Delta\nu = -\frac{1}{4\pi\rho}\oint ds\ \beta(s)\sum_n b_n(s)x(s)^{n-1} \tag{4.23}$$

The analysis then proceeds as before. Assuming uncorrelated contributions from the different magnets (even more dangerous here??), and taking a single term in the sum,

$$\langle(\Delta\nu_n)^2\rangle = \frac{1}{16\pi^2\rho^2}\,N_{mag}\,L_{mag}^2\langle b_n^2\rangle\langle\beta^2x^{2n-2}\rangle \tag{4.24}$$

Recalling that $\langle x^2\rangle = \frac{1}{2}\langle\beta\varepsilon\rangle^2$, we get, roughly

$$\sqrt{\langle(\Delta\nu_n)^2\rangle}_{rms} \sim \frac{\beta}{4\sqrt{2}\,\pi\rho}\sqrt{N_{mag}}\,L_{mag}\sqrt{\langle b_n^2\rangle}_{rms}\langle\beta\varepsilon\rangle^{\frac{n-1}{2}} \tag{4.25}$$

The scaling with energy follows, not surprisingly, the pattern we have seen before, and for higher moments (on paper) even improves, inasmuch as $\beta\varepsilon \sim E^{-1/2}$. The lower values of n, say 3 and 4, are contributed by sextupole and octopole fields, and are relatively controllable, inasmuch as such fields are deliberately included in the lattice to control chromaticity and help tame single-beam collective instabilities.

Higher orders in n are in less control.

The tune shifts (spreads) are very sensitive to large values of β, putting an especially high premium on field quality in the neighborhood of focussing quadrupoles.

5. Resonances

We have already seen that it is unwise to choose an integer for the machine tune inasmuch as dipole field errors drive resonances. Field errors of higher multipolarity drive higher order resonances at tune values, as we shall see, equal to an integer plus a vulgar fraction p/q, with p and q small integers. After the integer resonances, the simplest case is that of linear coupling resonances. These are contributed by tilted (skew) quadrupoles, for example.

$$\frac{d^2x}{ds^2} + k_x(s)x = \delta k(s)z$$

$$\frac{d^2z}{ds^2} + k_z(s)z = \delta k(s)x \tag{4.26}$$

Extension of the transfer-matrix method (to 4×4 matrixes) handles this case quite easily and exactly. The analysis is pretty.[15] It turns out that if

$$\nu_x + \nu_z = n \tag{4.27}$$

with n integer, there exists instability and emittance growth. For

$$\nu_x - \nu_z = n \tag{4.28}$$

there also exists resonance. Energy is transferred back and forth between horizontal and vertical motion in a manner similar to coupled degenerate pendula. But the betatron amplitudes remain bounded.

Nonlinear resonance phenomena are very rich and interesting. The dynamics of a single isolated nonlinear resonance can be worked through in a reasonably systematic way. To go beyond that point is to enter the active research field of 20th-century nonlinear mechanics. Here we shall only partially treat the case of a single nonlinear resonance. One begins with the perturbed Hill's equation

$$\frac{d^2z}{ds^2} + k(s)z = -\frac{1}{\rho}\sum_n b_n(s)z^n \tag{4.29}$$

and change variables ("Floquet transformation")

$$z = \sqrt{\beta(s)}\, v$$

$$d\phi = \frac{1}{\nu}\frac{ds}{\beta(s)} \quad (0\leq\phi\leq 2\pi \text{ around the ring}) \tag{4.30}$$

This smooths out the betatron motion into that of a harmonic oscillator:

$$\frac{d^2v}{d\phi^2} + \nu^2 v = -\frac{\nu^2}{\rho}\sum_n \beta(s)^{\frac{3+n}{2}}\, b_n(s)v^n$$

$$= -\sum_n \left(\sum_p A_p^{(n)} \cos p\phi\right)v^n$$

$$= -\sum_n A^{(n)}(\phi)v^n \tag{4.31}$$

The nonlinear term on the right-hand side is periodic in ϕ and drives the resonance. The above equation can be obtained from the Hamiltonian (think of ϕ as time!)

$$H = \frac{p^2}{2} + \frac{\nu^2 v^2}{2} + \sum_n \frac{A^{(n)}(\phi)}{n+1} v^{n+1} \tag{4.32}$$

The conventional method of solution starts with this Hamiltonian and performs successive canonical transformations until the dominant component of the nonlinearity (for given tune choice) is isolated. The remaining piece of the nonlinear Hamiltonian is then thrown away and the solution obtained by additional canonical transformations.

Nowadays the techniques of Hamiltonian mechanics are more familiar to many of us in the context of the quantum theory. We shall use that language here to motivate the procedure. The nonlinear term contains, in terms of creation and destruction operators a and a^+, terms of order $(a^+)^{n+1}$, inducing transitions with $\Delta E=(n+1)\nu$. The driving term $A_n(\phi)$ contains only integer fourier components exp $\pm ip\phi$. If the energy p of a quantum delivered by the driving term equals the excitation energy ΔE of the oscillator, there will be resonance

$$p = (n+1)\nu \tag{4.33}$$

or

$$\nu = \frac{p}{n+1} = \text{vulgar fraction} \tag{4.34}$$

Note that n is determined by the multipolarity of the magnetic field:

n = 1 quadrupole
2 sextupole
3 octupole
. .
. .
. .

while the resonance is driven (essentially)* by the p'th (circumferential) harmonic of the nonlinear force around the ring.

For coupled resonances, the Hamiltonian contains terms which have the form

$$H' \sim z^{n+1} x^{m+1} \tag{4.35}$$

These contain terms $\sim(a_z^+)^{n+1}(a_x^+)^{m+1}$, which by the previous argument gives the resonance condition

$$p = (n+1)\nu_z + (m+1)\nu_x \tag{4.36}$$

There can also be difference resonances (n,m,p integer) as well as sum resonances, driven by terms $\sim(a_z^+)^{n+1}(a_x)^{m+1}$. In this case, when the z oscillator is excited, the x oscillator is simultaneously de-excited. This is a relatively inefficient way to pump energy into the betatron-oscillators, and we infer that, in general, <u>sum resonances will be more dangerous than difference resonances.</u>

To get some more detailed insight into the nature of these resonances, we return to the uncoupled case of a pure sextupole term (n=2) in the oscillator calculation Eqn. (4.31). We expect

*The irregularity of the focussing structure (i.e. β- function) also contributes to the driving term.

that the following steps will set up the simplified calculation.

1. The resonance will be important when $\nu \equiv N+1/3$ or $N+2/3$, N integer, implying $p=3N+1$ or $p=3N+2$.

2. We shall find the equation of motion for the creation operator a^*, which we define as usual

$$v = \frac{1}{\sqrt{2\nu}} (ae^{-i\omega\phi} + a^*e^{i\omega\phi})$$

$$p = i\sqrt{\frac{\nu}{2}} (ae^{-i\omega\phi} - a^*e^{i\omega\phi}) \tag{4.37}$$

where we anticipate the need to remove some "time"-dependence (Remember! "time" is ϕ) from a^* by putting in the $e^{i\omega\phi}$ factor. The frequency ω will be chosen later; it will be approximately — but not precisely — equal to the natural frequency ν.

3. On the right-hand side, we keep only the term proportional to $e^{-ip\phi} a^2$, because that is the only one which will approximately match the frequencies and produce the resonance condition, Eqn. (4.33).

Then the equation of motion for a^* is easily found to be

$$\frac{da^*}{d\phi} = -i(\nu-\omega)a^* - A_2 e^{-ip\phi} e^{i3\omega\phi} a^2 \tag{4.38}$$

We choose

$$\omega = \frac{p}{3} \equiv \nu_{res} \tag{4.39}$$

to rid the equation of oscillatory factors and finally obtain

$$\frac{da^*}{d\phi} = -i(\nu-\nu_{res})a^* - A_2 a^2 \tag{4.40}$$

Now complex a-space is essentially rescaled phase-space. We see the following features:

1. The phase-space trajectories have a 3-fold symmetry; if $a(\phi)$ is a solution, so also is $a(\phi) \exp(2\pi i M/3)$ with M integer.

(For the generic $n^{\underline{th}}$ nonlinear term, this clearly generalizes to an (n+1) -fold symmetry.

2. There exist fixed points, i.e. "time-independent" solutions of $da/d\phi=0$. They satisfy

$$a^3 = -i\,\frac{\Delta\nu}{A_2} \tag{4.41}$$

and are at a distance from the origin given by

$$|a| = \left(\frac{\Delta\nu}{A_2}\right)^{1/3} \tag{4.42}$$

That is, they are far away unless

$$\Delta\nu \lesssim A_2 \tag{4.43}$$

which is, roughly, the condition on tune shift obtained earlier (Eqn.4.23).

3. On resonance, when $\Delta\nu=0$, the fixed points converge to the origin. One may then find simple radial solutions of the equation of motion. Writing

$$a(\phi) = \rho(\phi)e^{i\alpha} \tag{4.44}$$

with the phase α kept constant, we get

$$\frac{d\rho}{d\phi} = A_2 e^{3i\alpha}\rho^2 \tag{4.45}$$

For self consistency, we need $d\rho/d\phi$ to be real so that we must have

$$e^{3i\alpha} = \pm 1 \tag{4.46}$$

which gives six solutions for α, corresponding to rays emanating from the origin at $\theta=0^0$, 60^0,... Motion on three of the rays will be outward from the origin, and inward on the other three. In between these rays it is easy to guess the phase-space trajectories (Fig. 9a). The rays are clearly separatrices. [For nth-order resonance there are 2(n+1) such separatrices.]

4. Moving back off-resonance, the phase-space trajectories near the origin will be circular, oscillator like. Far from the

origin, well beyond the fixed points, the small change in tune will not affect the motions we deduced for the on-resonance case. Thus, in between there must be other separatrices linking the fixed-points. The final picture is as in Fig. 9b. For n=2 the separatrices turn out to be straight lines as shown. This is not true for higher n, although the basic geography — with periodicity n+1 instead of 3 — is the same as we have described.

Often there will be other focussing forces of higher multipolarity present. For example if there is a zero-harmonic octupole component which dominates the sextupole component at large amplitudes the outer separatrices will become closed, creating "islands of stability" (Fig. 14). This is a common pattern for the phase-space structure.

In the case of coupling resonances, a similar analysis can be made. For a generic interaction term

$$H' \sim (\cos p\phi) z^{n+1} x^{m+1} \sim e^{-ip\phi} (a_z^+)^{n+1} (a_x^+)^{m+1} \qquad (4.47)$$

the frequencies ω_z and ω_x must satisfy

$$p = (n+1)\omega_z + (m+1)\omega_x \qquad (4.48)$$

in analogy to Eqn. (4.39). It is convenient to also choose

$$\frac{\omega_z - \nu_z}{n+1} = \frac{\omega_x - \nu_x}{m+1} \qquad (4.49)$$

in order to obtain fixed-points in the 4-dimensional a_z-a_x phase space. (These "fixed"-points actually are one-dimensional paths.) We shall, however, not go further into describing the structure of this phase space.

One should not get the idea that we have even begun to cover the fascinating topic of nonlinear resonances. The phase space structure is extremely rich — in fact fractal. Some idea of this richness can be gleaned by looking at computer- generated iterated maps — now nonlinear — for even simple nonlinear motions in 2-dimensional phase space.[16] One starts with a few particles at some initial points $(x_i(s_0), x_i'(s_0))$, compute (including nonlinear forces) their positions $(x_i(s_0+NC),\ x_i'(s_0+NC)$ after $N=1,2,\ldots 10^{5\pm1}$ revolutions and then plots all the resultant phase points (Fig. 11).

In regions of stability one sees reasonably deterministic orbits. Near separatrices one sees "stochastic layers" emanating from the unstable fixed points. If one recalls the nature of the most elementary unstable fixed point — a pendulum balanced at maximum amplitude — one may appreciate that when a phase point finds itself near an unstable fixed point its future is vitally dependent on the details of small perturbations in the present and tends toward indeterminacy.

But within chaos lies order. Upon looking with a magnifying glass at stochastic regions, one finds more islands of stability with their own fixed points and stochastic layers, <u>ad infinitum</u>.* And all this structure is found in a one (space) dimensional system. Essential complications occur in higher dimensions.[16]

We may summarize all these anxious estimates of instabilities in terms of a tune diagram (Fig.12). The lines show danger zones from low order resonances. The <u>operating point</u> (really a small area) must be judiciously chosen to avoid the important resonances. There are exceptions: Nonlinear resonances, deliberately stimulated, are used to slowly extract a beam from an accelerator.[17] Also, we may need the resonances in the 2020 machine to blow up the beam to keep a manageable current density (low beam-beam tune shift) at high current.

V. MACHINE PARAMETERS

The main parameters of the 2020 machine are shown in Table I. We have included, for comparison, various numbers from the CERN PS, Fermilab Tevatron, and the 20 TeV ICFA machine (VBA). We now comment in turn on the choice of parameters in those cases where it is not obvious from what has been directly presented. Beware! None of the numbers are consistent to more than 20%.

1. The magnet lengths are chosen as 7m, which is the state-of-the-art. The 10T field for dipoles and 2T/cm for quads is not state-of-the-art, but is assumed by ICFA as state-of-the-art for the 20 TeV machine. Therefore we use it. The choice of tune is somewhat arbitrary, and is based on the fraction of circumference in quadrupoles, ℓ/L, chosen to be 10%, somewhat larger than the custom, but not the maximum which might be contemplated on economic grounds. With $\ell/L=0.1$, Eqn. (3.45) yields for the half-cell length L

*Not infinitum! Quantum mechanics soon intervenes.

$$L^2 = \sqrt{2}\,\frac{B\rho}{G}\left(\frac{L}{\ell}\right) = (340\text{m.})^2 \tag{5.1}$$

Dividing into the circumference gives the number of cells, and thereby the tune, which is 1/4 the number of cells. (Remember, betatron phase advance/cell is 90°.)

To obtain the maximum and minimum values of β in the normal lattice, we use Eqn. (3.38) directly. Likewise, the nominal value of the dispersion (or off-momentum) function $\langle\eta(s)\rangle$, and "dilation factor" η is found from Eqns. (3.56) and (2.41).

2. Collision Region

Thus far, we have not inserted straight sections into the regular lattice of the machine. These are required for beam injection, beam abort, and RF, as well as for the collision regions.

a. β and β' should be matched at the input and output of the straight section in order that the optics of the rest of the machine not be disturbed. This typically implies an integer contribution of the insertion to the tune.

b. It is deemed desirable to design the insertion region so that the dispersion function $\eta(s)$ in the straight section vanishes. The most straightforward way to change η in some region is to add an opposed pair of dipole doublets as shown in Fig. (13). But this is unnecessarily elaborate; it suffices to decrease (by a factor ~2) the bending strength of the dipoles in the cells adjacent to the straight sections to accomplish the goal.

In the collision straight-sections, one naturally wants to focus the beams especially strongly, i.e. reduce the β-function at the collision point to a small value. One (or more) pairs (or triplets) of strong, large-aperture quadrupole magnets are utilized for this purpose. The rough behavior of the β-function in the straight section is shown in Fig. (14). The β-function in a drift space has a quadratic behavior:

$$\beta(s^*+\ell) = \beta^* + \frac{\ell^2}{\beta^*} \tag{5.2}$$

where ℓ is the distance from the collision point s^*. [To see this observe that the transport matrix for one revolution starting a distance ℓ from s^* is

$$M(s^*+\ell+C,s^*+\ell) = \begin{pmatrix} 1 & \ell \\ 0 & 1 \end{pmatrix} \begin{pmatrix} \cos 2\pi\nu & \beta \sin 2\pi\nu \\ -\beta^{-1} \sin 2\pi\nu & \cos 2\pi\nu \end{pmatrix} \begin{pmatrix} 1 & -\ell \\ 0 & 1 \end{pmatrix} \qquad (5.3)$$

Calculation of the upper right hand element produces Eqn. (5.2)).]

Thus the maximum value of β, which we call $\hat{\beta}$, occurs in the neighborhood of the final focussing quadrupoles, is roughly

$$\hat{\beta} = \frac{\ell^{*2}}{\beta^*} \cong \frac{(L_{straight} - \ell^*)^2}{\langle\beta\rangle} \qquad (5.4)$$

where $\langle\beta\rangle$ is a typical (or slightly less-than-typical) value of β in the normal lattice. For $\beta^* \ll \langle\beta\rangle$, $L_{straight} \gg \ell$, and

$$L_{straight} \sim \sqrt{\langle\beta\rangle\hat{\beta}}$$

one has

$$\ell^* \sim \sqrt{\beta^*\hat{\beta}} \qquad (5.5)$$

The maximum allowed β is determined by aperture limitations of the quad, focal power (the length of the doublet must be less than ℓ^*), and chromaticity. Inspection of Eqns. (3.62) and (3.40) show that, in the very-strong focussing limit of phase advance of ~180°/cell, a single doublet in the lattice contributes an amount $\delta\xi$ to chromaticity of

$$d\xi \sim \frac{1}{\nu} \sqrt{\frac{\beta_{max}}{\beta_{min}}} \qquad (5.6)$$

With 4 collision regions (and two quad pairs per straight section) we should have

$$\frac{8}{\nu} \sqrt{\frac{\beta_{max}}{\beta_{min}}} = \frac{8}{\nu} \sqrt{\frac{\hat{\beta}}{\beta^*}} \ll 1 \qquad (5.7)$$

in order that the natural chromaticity not be dominated by interaction-region quads. Thus we guess

$$\frac{\hat{\beta}}{\beta^*} = \frac{\beta_{max}}{\beta_{min}} \lesssim 500 \tag{5.8}$$

Guessing

$$\begin{aligned} \hat{\beta} &= 10 \text{ km} \\ \beta^* &= 20 \text{ m} \\ \langle\beta\rangle &= 500 \text{ m} \end{aligned} \tag{5.9}$$

gives

$$\begin{aligned} \ell^* &= 100 \text{ m} \\ L_{straight} &= 2.5 \text{ km} \end{aligned} \tag{5.10}$$

These estimates are very superficial, and may be quite wrong. Some clues on how to do better may be found in discussions by Keil.[18]

In some machines, one must also ensure, because of the behavior, Eqn. (5.2), of β near the collision point, that the bunch length not exceed β^*. This is evidently not a problem in the 2020 machine.

3. RF System and Synchrotron Radiation

These have already been discussed, and we have nothing much to add here. Because of the problems with the collective, single-beam instabilities one might want to increase bunch length by lowering the RF frequency. This would allow, according to the Keil-Schnell criterion, Eqn. (2.77), more protons per bunch. For a more-or-less uniformly filled RF bucket, the bunch length and hence the number of protons in the bucket is inversely proportional to the RF frequency.

4. Injection

Superconducting magnets exhibit a kind of hysteresis associated with persistent currents generated in the superconducting wire. This limits the injection field to >10-20% of the peak field. Thus a reasonable injection energy is ~70 TeV. This implies that the 2020 machine would probably be third generation: 1TeV → 10TeV → 70TeV → 500TeV. At injection energy the beam emittance will be larger by a factor ~7, and beam size by a factor ~2-3, than at peak energy. Thus, unlike what we have done, tolerances are typically most severe for injection conditions. This will not affect our estimates of how tolerances scale with energy, inasmuch as the ratio of injection to peak energy is, to first order, independent of machine.

We have neither addressed the question of how beam is injected nor how it is aborted, i.e. extracted in no more than one turn if trouble is sensed. This is done with pulsed magnets (kickers); I see no epic problems in doing that, although in the case of aborts the demands on beam dump design may be heavy.

5. Beam Parameters

The emittance of the FNAL machine at transition (~20GeV) is $\epsilon \sim \pi$ mm-mrad. The quoted numbers for the 2020 machine are scaled up by the E^{-1} factor implied by Liouville's theorem. They should be considered as roughly 2σ estimates, unless otherwise stated. This incudes the longitudinal emittance.

We should not take seriously the beam parameters after synchrotron- radiation damping. They are only relevant for low intensity beams. We shall instead assume bunches of 5×10^{11} particles which are "artificially" maintained at an optimal transverse size by, say, occasionally tuning onto an appropriate resonance to blow up the beam. Likewise we assume the RF buckets can be uniformly filled either by manipulations at injection and/or by using the microwave instability itself.

6. Limits from Single-Beam Instability

We shall assume that the principal limitation on bunch intensity comes from the longitudinal "microwave" instability which we have already treated in Section II.7. We shall take the "long bunch" case, with rms bunch length σ_s=10 cm. This produces an rms momentum spread of order $\sigma_p \cong 30$ GeV or $\sigma_\eta = \sigma_p/p \cong 6\times10^{-5}$. The Keil-Schnell criterion, Eqn. (2.77), for these parameters gives, for $Z_{||}/n \sim 3$ ohms and $\Delta p = 2\sigma_p \sim 60$ GeV, a limiting peak current of $i_{peak} \leq 100$ ampere. With

$$i_{peak} \simeq \frac{N}{\sqrt{2\pi}\sigma_s} \qquad (5.11)$$

this implies

$$N \leq 5 \times 10^{11} \qquad (5.12)$$

As shown in the Supplement, we may hope to put one bunch per betatron wavelength into the machine; this would imply ~400 bunches, or ~2×10^{14} p and $\bar{p}$ stored in the ring. This in turn requires an improvement in antiproton production by a factor 10^2-10^3 over existing sources. [If necessary, this problem could be overcome by building ~100 sources; this would not peturb greatly the total cost of the machine!!]

7. Luminosity

The formulae for luminosity and beam-beam tune-shift differ sightly from the rough estimates we have previously used, if one considers gaussian beams. We use (compare with Eqn. (2.81))

$$= \frac{N_p N_{\bar{p}} n_b}{4\pi\sigma_x^*\sigma_z^*}\left(\frac{\omega_0}{2\pi}\right) \qquad (\sigma_z \ll \sigma_x) \tag{5.13}$$

where

N_p = No. of protons per bunch

n_b = No. of bunches in ring

$\sigma_{x,z}$ = rms beam size at collision point (5.14)

The vertical beam-beam tune shift per crossing $\Delta\nu$ is, instead of Eqn. (2.85),

$$\Delta\nu \equiv \frac{\alpha N \beta_z^*}{2\pi E_p \sigma_x^* \sigma_z^*} \qquad (\sigma_z \ll \sigma_x) \tag{5.15}$$

We shall assume that the beams are separated except in the four collision regions. This is discussed in the Supplement; electrostatic deflectors are used to separate the beams except at collision points. We shall furthermore assume that the beam-beam effects from different collision regions add incoherently, so that $\Delta\nu \sim \sqrt{N_{\text{crossings}}} = \sqrt{8}$. There is little theoretical justification for this, although it is not too bad empirically.

The strategy is therefore fixed:

a) $N_{p,\bar{p}}$ is determined by the limit on beam current from longitudinal microwave instability.

b) β_z^* is minimized via lattice-optics considerations.

c) $\sigma_x^*\sigma_z^*$ is determined by the condition (good to factor ~3!!)

$$\Delta\nu = .01 \tag{5.16}$$

It will be larger than the natural value from synchrotron damping. Putting numbers into Eqn. (5.15) gives

$$\sigma_x^* \sigma_z^* = 8 \times 10^{-6}\ \mathrm{cm}^2 \tag{5.17}$$

Assuming $\sigma_x^* = 2\sigma_z^*$ for definiteness gives for emittance

$$\frac{\varepsilon}{\pi} = \frac{(2\sigma_z^*)^2}{\beta^*} \sim 20\ \mu\mathrm{m}\text{-}\mu\mathrm{rad} \tag{5.18}$$

This is only slightly less than what exists immediately after injection and acceleration. We must assume that the beam can be artificially excited and the size controlled.

This problem exists already in e^+e^- storage rings. It has proved difficult to blow up the transverse phase space by external means; the synchrotron damping dominates. However, in those cases the damping time is of order milliseconds instead of a fraction of an hour, so the problem for the 2020 machine may not be as severe. Mechanisms for enlarging the phase space might be tuning onto weak betatron resonances or adding RF noise.

d) With n_b of order ν, as determined by the scheme for electrostatic separation of the beams, we may now directly estimate the luminosity. We obtain

$$\mathscr{L} = 10^{33}\ \mathrm{cm}^{-2}\ \mathrm{sec}^{-1} \tag{5.19}$$

and per crossing

$$\mathscr{L} = 10^{28}\ \mathrm{cm}^{-2}/\mathrm{crossing} \tag{5.20}$$

There is a lot of uncertainly in this estimate. A tune shift per crossing of .005 may be too big by a factor 2-3. This influences linearly the luminosity. Putting 5×10^{11} particles in a short bunch may be overoptimistic. The diminution in luminosity goes linearly with N (provided the beam-size at the collision point can be re-optimized).

But perhaps the most severe constraint comes from detection problems. There are, with this luminosity, many interactions per crossing. These cannot be resolved by existing detection techniques, and thus the physics opportunities are constrained. These problems are discussed in the next section.

VI. DETECTION PROBLEMS

A traditional design requirement for colliders is that there be no more than one interaction per bunch crossing. This implies, for a total cross-section (within factor 2) ~10^{-25} cm^2, a luminosity per crossing ~$10^{25}cm^{-2}$. Furthermore, we have seen that the bunch spacing for a $p\bar{p}$ collider is (optimistically!) ~ one bunch per betatron wavelength. Since the betatron wavelength increases with energy this implies (using these ground rules) that the net luminosity is ~

$$\mathcal{L} = 10^{25}\ \nu\ \frac{\omega_0}{2\pi} \tag{6.1}$$

For the 2020 machine with ν~400 and $\omega_0/2\pi$=250 sec^{-1}, this gives

$$\mathcal{L} \sim 10^{30} cm^{-2} sec^{-1} \tag{6.2}$$

which is hardly adequate for investigation of hard collisions with subprocess cross-sections (at the energy scale appropriate to this machine (~10-300 TeV), which may be estimated (just from dimensional analysis) to be

$$\sigma \le \frac{1}{s} \tag{6.3}$$

i.e.

$$\sigma \le (4\times10^{-36}\text{ to }4\times10^{-39} cm^2) \tag{6.4}$$

If one allows multiple collisions per crossing, one cannot expect charged particle tracking or-at these energies - even muon identification to be viable. One is left with electromagnetic and hadron calorimetry. In the case of calorimetry, a certain amount of pileup can be tolerated without losing too much information. The situation is described in more detail in the Supplement. Here we summarize a few of the salient points. First of all, we can only hope to see very high p_T jets. In principle calorimeter resolution for energies above 1 TeV is not much of a problem, although the clean isolation of a hadronic jet in the presence of QCD gluon bremsstrahlung may be a considerable nuisance. We now estimate the pileup underneath an observed high-p_T jet. First of all we assume the jet is contained within 0.1 steradian. The distribution of energy into 0.1 steradian (at 90^0 cms) is empirically bounded above by an exponential

$$\frac{dN}{dE_T} \le \frac{c}{\langle E_T\rangle}\ e^{-\frac{E}{\langle E_T\rangle}} \tag{6.5}$$

with $\langle E_T\rangle$ an increasing function of total cms energy. The value of $d\langle E_T\rangle/d\Omega$ versus energy is shown in Fig. 15. The value at $\sqrt{s}$ ~ 10^3 TeV might be as large as ~5 GeV/steradian. Then 1000 collisions per bunch crossing could put, <u>on</u> <u>average</u>, 500 GeV into each calorimeter element subtending 0.1 steradian. The fluctuations about the average, however, are bounded above by a Poisson distribution.

$$\frac{dN}{dE_T} \leq \frac{1}{N!}\left(\frac{cE_T}{<E_T>}\right)^N e^{-\frac{E_T}{<E_T>}} \qquad (6.6)$$

For $E_T >> N<E_T> = 10^3 \times 0.5$ GeV the exponential is dominant and leads to negligible background. Thus a threshold jet energy in the range 1-3 TeV is very reasonable. There thus remains a hope to reconstruct multijet systems provided only the total mass of the system and subsystems is very large compared to, say, 3 TeV. But that is, after all, the main reason to build such a high energy collider in the first place.

VII. CONCLUDING COMMENTS

Within the limitations of this study, as carried out by an inexperienced amateur, there is no evidence that this monster of a machine does not work, with luminosity adequate to do the physics it naturally addresses. Detection problems are demanding because of pileup, but should not be insurmountable. There are evident practical problems. Not only is there a funding problem, but also a system problem. Not one of the 2×10^5 cantankerous superconducting magnets and their complex support systems can fail. This question of quality control might well be the most demanding technical problem of all.

Various problems of this machine were addressed by participants of the school. These included the question of disposal of synchrotron radiation (use warm "scrapers" located between magnet strings), beam abort systems (conventional methods seem to work), the electrostatic deflection system to keep p and $\bar{p}$ bunches from colliding except in interaction regions, and detection problems associated with multiple interactions per bunch crossing. These latter two topics are included here in two supplements.

A major omission in these lectures is an adequate discussion of single-beam instabilities. The reader is urged to consult the references in Appendix I for more information, in particular A. Chao (ref. A7, SLAC School), C. Pellegrini (ref. A7, Fermilab School), and A. Hofmann et.al. (ref. A4, Erice School).

We thank T. Ferbel for his skillful organization of this school, and the participants for help and criticism in the preparation of this material. We thank also L. Teng for helpful criticism.

APPENDICES

I. Reference Material

There is considerable material on high energy accelerators and storage rings, ranging from textbooks to monographs and lecture series, to published papers, and to preprints and internal laboratory memoranda. (The latter component often seems to be the dominant one!) I am not enough of a scholar to provide an authoritative bibliography, but shall simply list here a few which were used in preparation of these notes. This listing should provide the reader with an avenue into more detaled papers on specific topics.

REFERENCES

A1. H. Bruck, "Circular Particle Accelerators," PUF, Paris (1966). A good general reference. (Unfortunately the only copy I could locate was in French.) Translated by LASL LA-TR-72-10 Rev.

A2. M. Sands, SLAC report SLAC-121; also "Physics with Intersecting Storage Rings," ed. B. Touschek, Academic Press, N.Y. 1971. This is a splendid introduction to e^+e^- rings and especially problems of synchrotron radiation.

A3. E. J. N. Wilson, CERN 77-7, "Proton Synchrotron Accelerator Theory." CERN academic-training lectures; a very nice introduction.

A4. "Theoretical Aspects of the Behavior of Beams in Accelerators and Storage Rings," CERN 77-13. A quite comprehensive discussion of many topics at a fairly advanced level. (This is the proceedings of an Erice school on accelerators.)

A5. Proceedings of the ICFA Workshops on Possibilities Limitations of Accelerators and Detectors. The first (1978) is a Fermilab report; the second (1979) a CERN report. These consider design problems of very big (e.g. 20 TeV) rings and are very useful source material for considering the 2020 machine.

A6. "Nonlinear Dynamics and the Beam-Beam Interaction," AIP Conference Proceedings No. 57. This nicely explores the interface between accelerator design and 20th century nonlinear mechanics.

A7. "Physics of High Energy Particle Accelerators," AIP Conference Proceedings No. 87 and No. xxx, ed. R. Carrigan, R. Huson, and M. Month. This contains the proceedings of a 1981 Fermilab Summer School. A second school was held at SLAC in 1982; proceedings have not yet appeared.

A8. "Techniques and Concepts of High Energy Physics," ed. T. Ferbel (Plenum, New York, 1981). This is the 1980 NATO Summer Institute Proceedings, and contains lectures by M. Month on specialized topics including beam-beam interaction and single-beam instabilities.

APPENDIX II: Limerick to a Theoexperimentalist

A well known theorist, Bjorken,
Field theory his great claim to fame;
Did an experiment one day,
Couldn't re-normalise away,
And something just snapped in his brain.

The result of this now must be
We henceforth accept G-U-T;
That theorists may change,
To plumbers ain't strange,
Especially at quadrillion eV.

Robert J. Wilson

APPENDIX III. The Missing Supplement

Regrettably the supplement mentioned in the text was unable to be completed. It was meant to consist of two parts. The material for the first, on bunch avoidance using electrostatic separators, was worked out by Nikos Giokaris. The scheme is practical and appears to cause no great difficulty, although it imposes geometrical constraints on the lattice design.

The material for the second part was provided by Geoffrey Taylor. It considers the interesting problem of detector design in the presence of multiple interactions per beam crossing. For jet transverse momenta well in excess of 1 TeV, problems of pileup appear to be small.

It was my intention to assist in editing and assembling this material together with the authors. But other pressures and commitments crashed in as the publication deadine approached, and there was no time available to properly complete the work. I deeply regret this failure and apologize to Nikos and Geoffrey, and thank them for their hard work.

REFERENCES

Note: Reference numbers preceded by an A are to be found in Appendix I.

1. See the discussions by L. Lederman and others at the 1982 Snowmass Summer Study.

2. For background see J. Bjorken, reference A7 (AIP. 92), p. 25.

3. For example, R. R. Wilson, Revs. Mod. Phys. 51, 259 (1979).

4. Particle Properties Data Booklet, Particle Data Group [Physics Letters 111B, (1982).

5. For example, A1, A3, A4.

6. See reference A2.

7. For example, see A. Piwinski, DESY Report M-81/03.

8. For example, se A. Chao, 1982 SLAC School, reference A7.

9. E. Keil and W. Schnell, CERN-ISR-TH-RF/69-48 (1969).

10. H. Hereward, Proc. of 1975 Isabelle Summer Study, p. 555.

11. A comprehensive review is given by J. Schonfeld, 1982 SLAC School, reference A7.

12. See E. Keil, Ref. A4.

13. See Ref. A3.

14. N. King, 2nd ICFA Workshop (Reference A5, Appendix I), p. 155.

15. See E. Courant, Fermilab Summer School (Reference A7, p. 1 AIP No. 87.

16. See contributions by R. Helleman and J. Moser, for example, in reference A6.

17. See for example L. Teng, reference A7 (AIP No. 87), p. 62.

18. E. Keil, reference A7 (AIP No. 87,) p. 405.

FIGURE CAPTIONS

1. The "Livingston plot" showing growth of attained cms energy of hadron machines versus time.

2. Typical betatron amplitude of a particle in a FODO lattice. Also shown is the amplitude function $\sqrt{\beta\epsilon}$ (cf. Section III).

3. Typical z-p_z phase-space population at various points in the FODO lattice (moving downstream): (a) At the center of an F (focussing) quadrupole, (b) Between F and D (defocussing) quadrupoles, (c) At a D quadrupole, and (d) Between D and F quadrupoles.

4. Closed orbit of an off-momentum particle in the FODO lattice.

5. Structure of longitudinal phase space for a bunched beam (in absence of acceleration and/or synchrotron radiation).

6. Structure of longitudinal phase space during acceleration (or in presence of synchrotron radiation).

7. "Invariant torus" for particles of a given emittance traversing a constant focussing structure.

8. Phase-space positions of particles of a given emittance at various locations in a FODO lattice. The curves are loci of constant emittance. Compare Figs. 3 and 8. (a) F quad, (b) between F and D, (c) D quad, and (d) between D and F.

9 Regions of z-p_z phase space near a 1/3-integer resonance: (a) on resonance, and (b) just off resonance.

10. Modification in presence of a zero-harmonic octupole component which produces stability at large amplitudes.

11. Iterated maps in presence of large nonlinearity. From Reference A6, pp. 232 and 285.

12. Tune diagram showing dangerous resonances.

13. Simple dispersion suppressor.

14. Schematic of optics in collision straight section.

15. Mean transverse energy into one steradian at 90° versus collision energy.

TABLE I: PARAMETER LIST††

	Scaling Rule	2020
Energy per beam	~E	500 TeV
Peak magnetic field	~B	10 T
Bending radius	~E/B	170km
Nominal circumference	~E/B	≳12600m
Dipole magnet Length		7m
Number of dipoles		170,000
Peak quadrupole Gradient	G	2T/cm.
Quadrupole Length		7m
Cell length	$\sim(EB/G)^{1/2}$	~700m
Betatron phase advance/cell		90°
Betatron tune (horizontal~vertical)	$(EG/B)^{1/2}$	400
Transition energy	$(EG/B)^{1/2}$	~400 GeV
Length of quads per half-cell		~35m
Number of quads per cell		10
Total number of quads		16,000
Maximum β	$(E/BG)^{1/2}$	~1200m
Minimum		~200m
Nominal dispersion $\langle\eta(s)\rangle$	$\sim G^{-1}$	0.7m
Momentum compaction η	(B/EG)	4×10^{-5}
No. of long straight collision regions		8

Full length of long straight section	$(EB/G)^{1/2}$	~3km
β* at collision point		~20m
Free space around collision point		±100m
Maximum β at quads		10km
Revolution frequency	B/E	250Hz
RF frequency		500Mhz
Harmonic number		2×10^6
RF voltage		5GeV
Synchrotron frequency		~1Hz
Maximum Δp		±150GeV
Maximum Δp/p		3×10^{-4}
Bucket area		~600 eV-sec
Synchrotron radiation energy loss/turn	$\sim E^3B$	3 GeV
Photon critical energy	$\sim E^2B$	300 keV
Longitudinal damping time	$\sim E^{-1}B^{-2}$	~10 min
Transverse damping time	$\sim E^{-1}B^{-2}$	~20 min
Injection energy		70 TeV
Transverse emittance		
at injection	E^{-1}	~300 μm-μrad
at peak energy*		~40 μm-μrad
Nominal rms beam size:		
at injection		~0.2 mm
at peak energy*	$(EBG)^{-1/4}$	~70μ

Nominal rms p_T-spread:		
at injection		±30 MeV
at peak energy*	$(EBG)^{1/4}$	±70 MeV
Longitudinal emittance at injection	~1	2eV-sec
Rms momentum spread Δp*	~1	±15 GeV
Rms $\Delta p/p$ at 500 GeV*	E^{-1}	$\pm 3\times 10^{-5}$
Rms bunch length*	~1	±3 cm
Nominal rms beam size+		
Horizontal	$(B^3/EG^2)^{1/2}$	20μ?
Vertical		2μ?
Emittance‡		
Horizontal	$(B^7/E^3G^3)^{1/2}$	1μm-μrad?
Vertical		10^{-2}μm-μrad?
Rms momentum spread‡		
Rms $\Delta p/p$	$(EB)^{1/2}$	$\pm 3\times 10^{-5}$
Rms bunch length‡		±3m
Rms beam size at collision‡		
Horizontal		4μ
Vertical		0.5μ
Optional rms beam size (500TeV)		
Horizontal		90μ
Vertical		90μ
Optimal rms emittance		
Horizontal		20πμm-μmrad
Vertical		20πμm-μmrad

Optimal rms momentum spread $\Delta p/p$	$\pm 6\times 10^{-5}$
Optimal rms bunch length	$\pm$5cm
Optimal rms beam size at collision	
Horizontal	40μ
Vertical	20μ
No. of $p(\bar{p})$ per bunch	5×10^{11}
No. of bunches	400
Beam-beam tune shift/crossing	.01
Luminosity	$10^{33}\text{cm}^{-2}\text{sec}^{-1}$
Energy stored in each beam	20GJ
RF power	200MW
Refrigeration power	3GW?

*Prior to synchrotron damping.
†At 500 TeV, dilute beam, after synchrotron damping.
††The parameters for ICFA, TeV I, and PS were hard for me to assemble and verify. They have been dropped for the table.

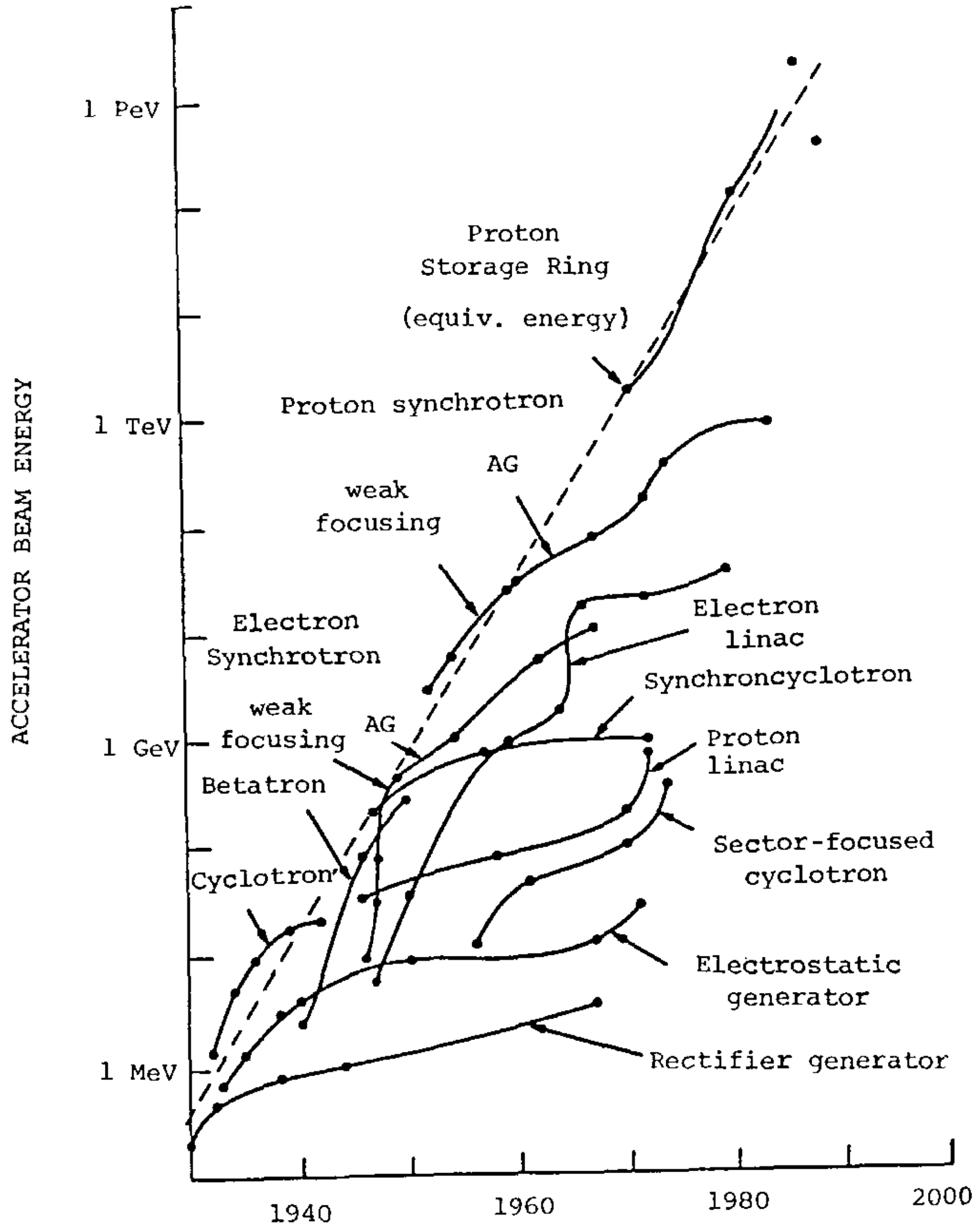

Figure 1

Fig 1

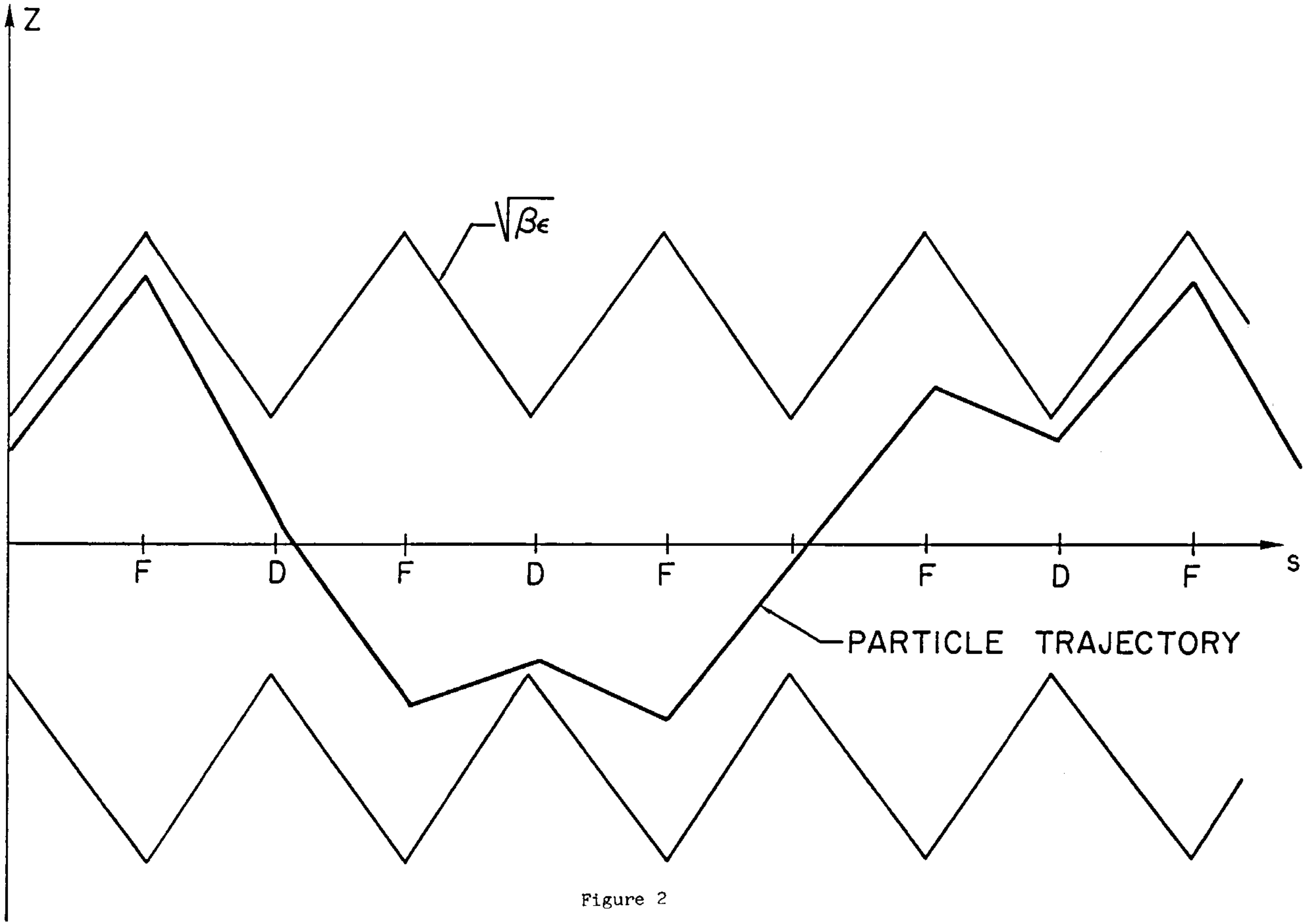

Figure 2

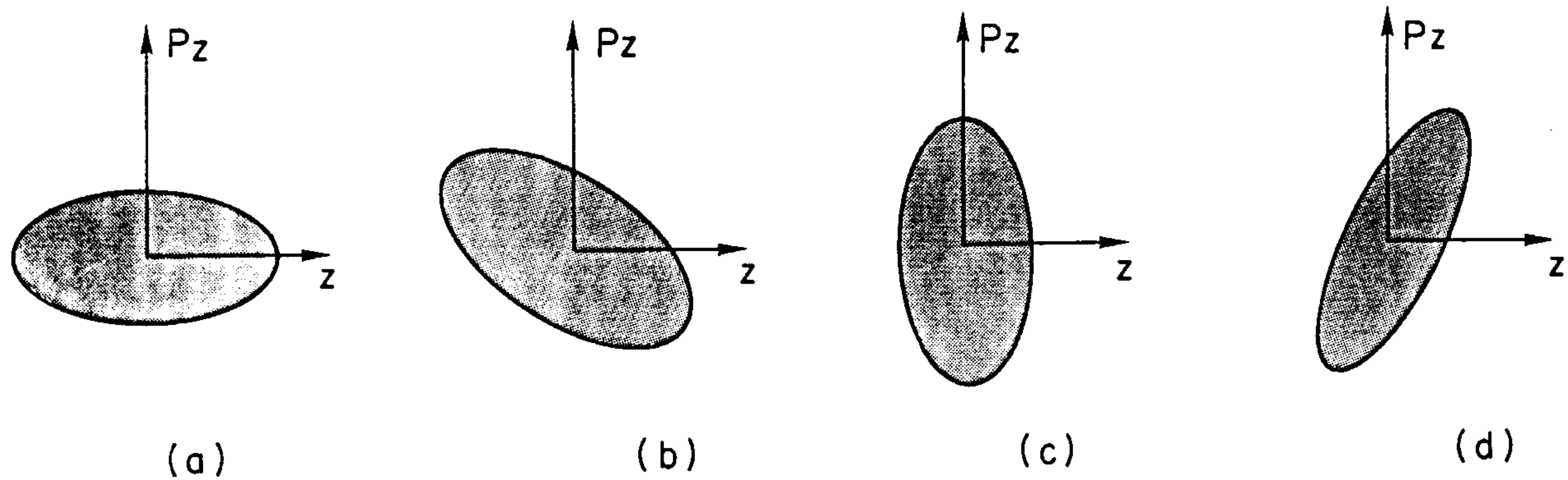

Figure 3

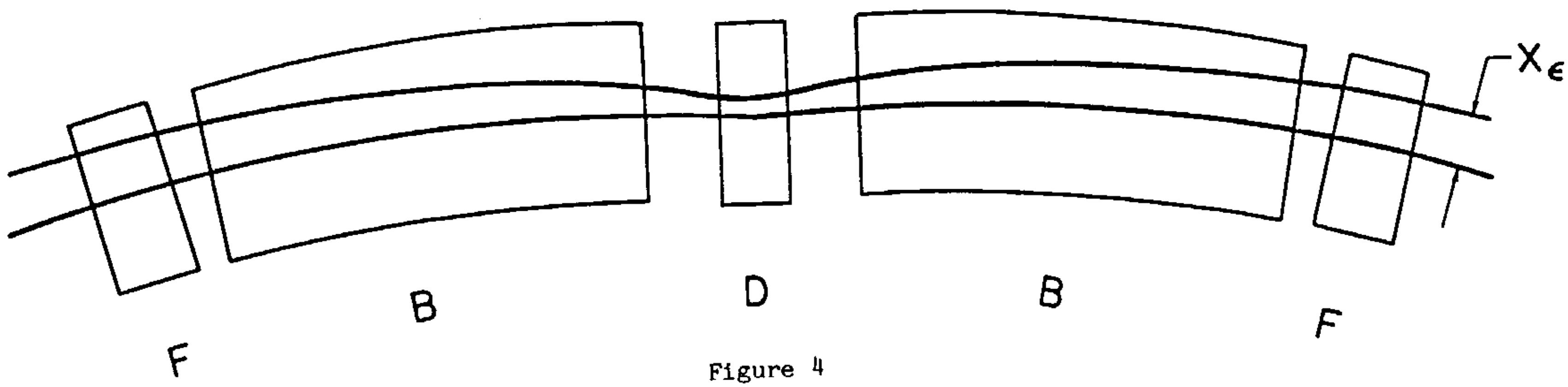

Figure 4

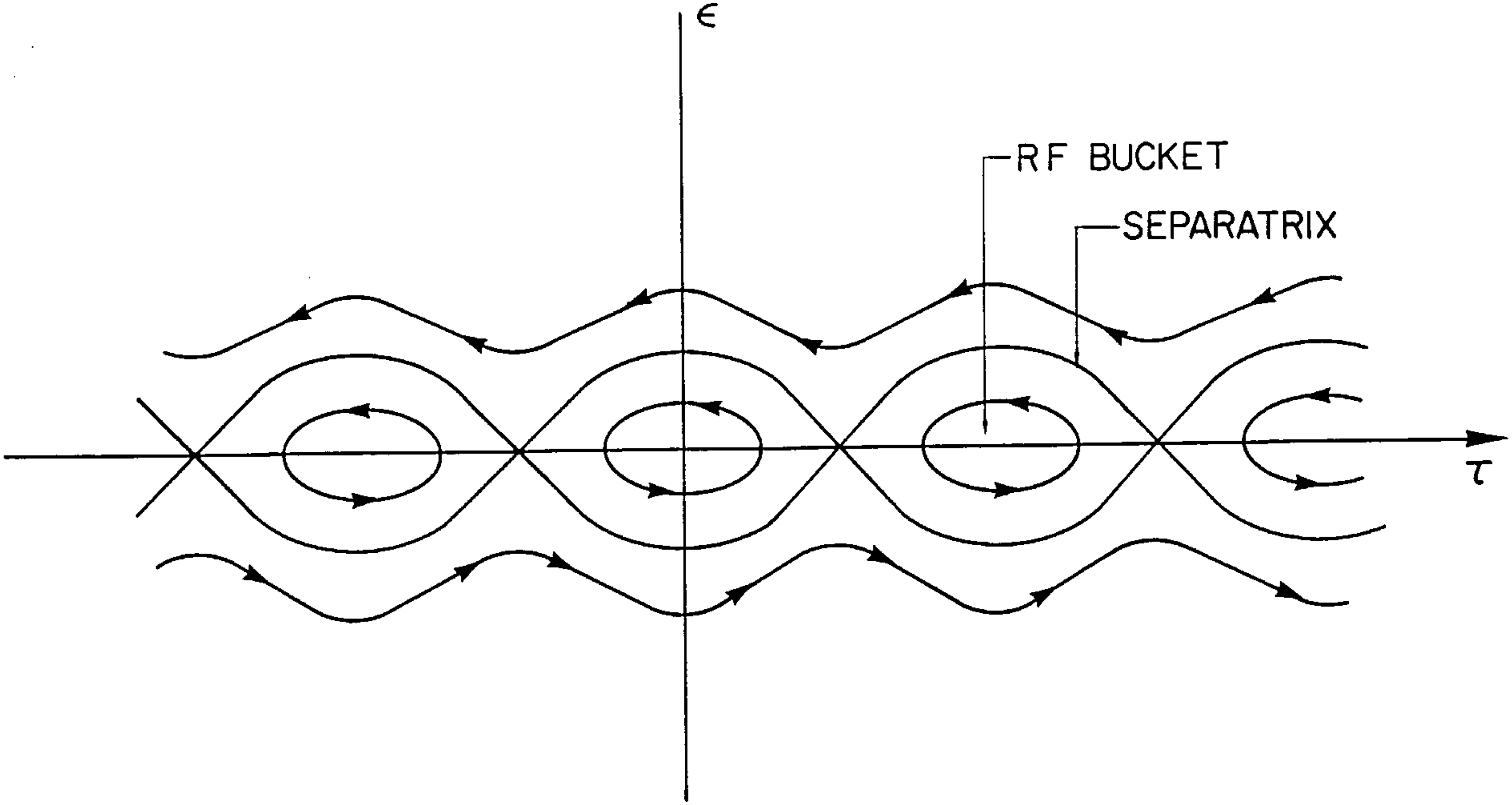

Figure 5

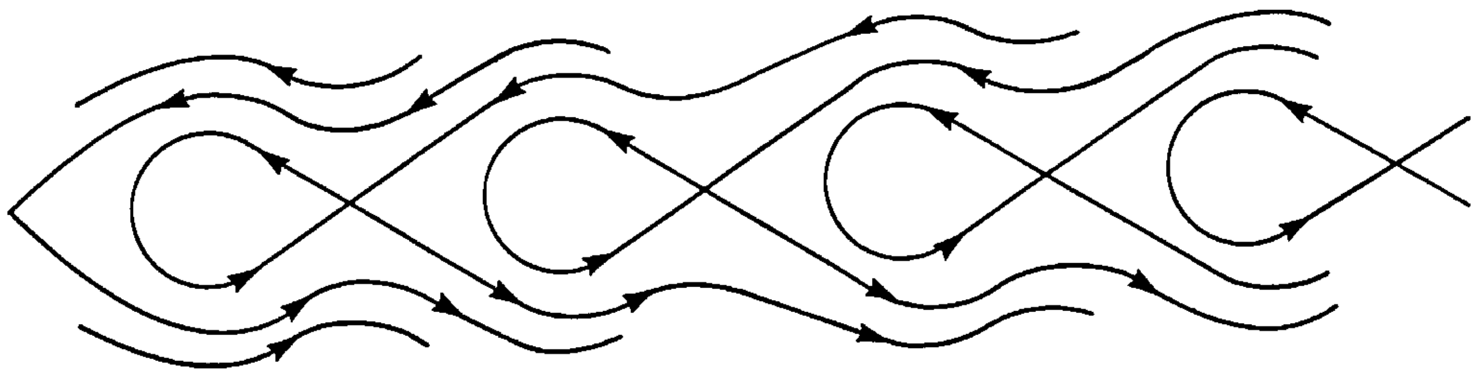

Figure 6

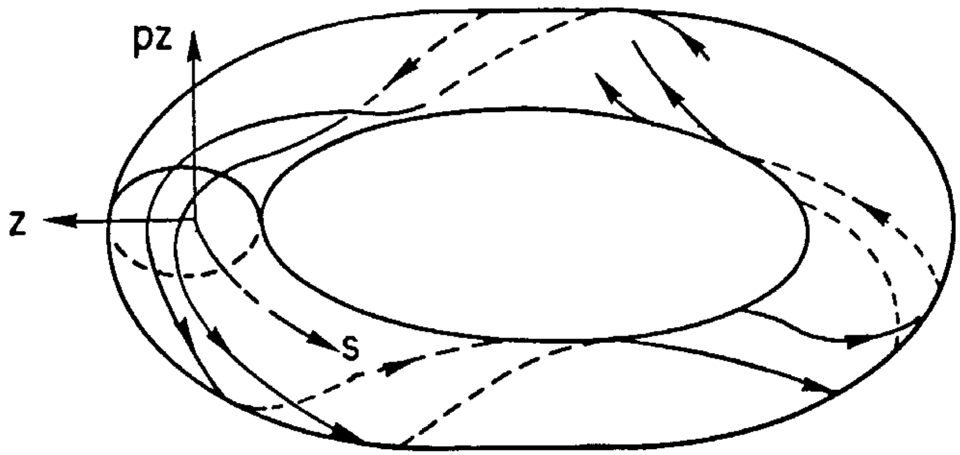

Figure 7

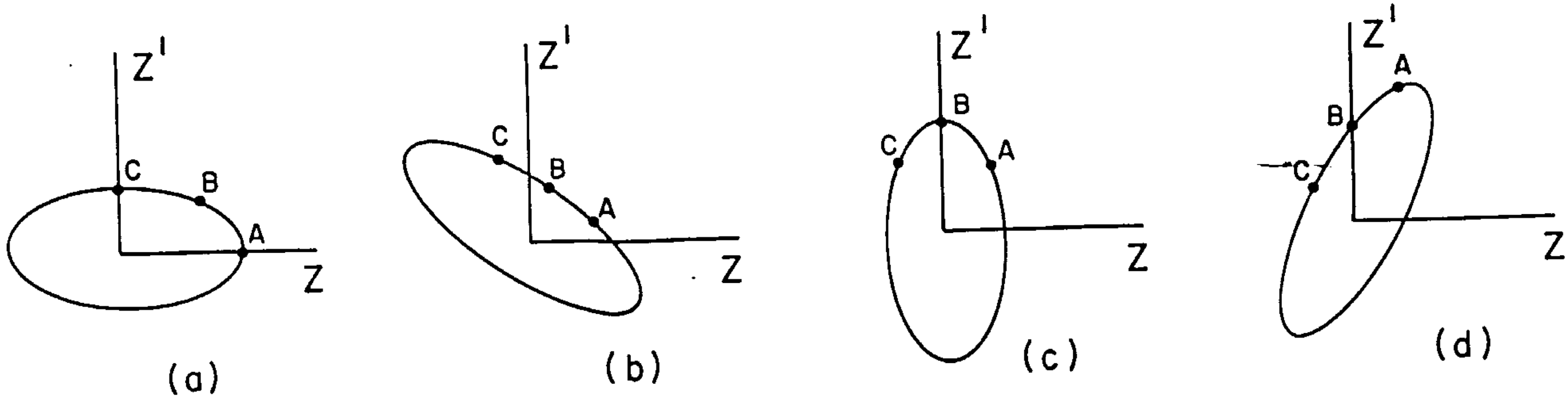

Figure 8

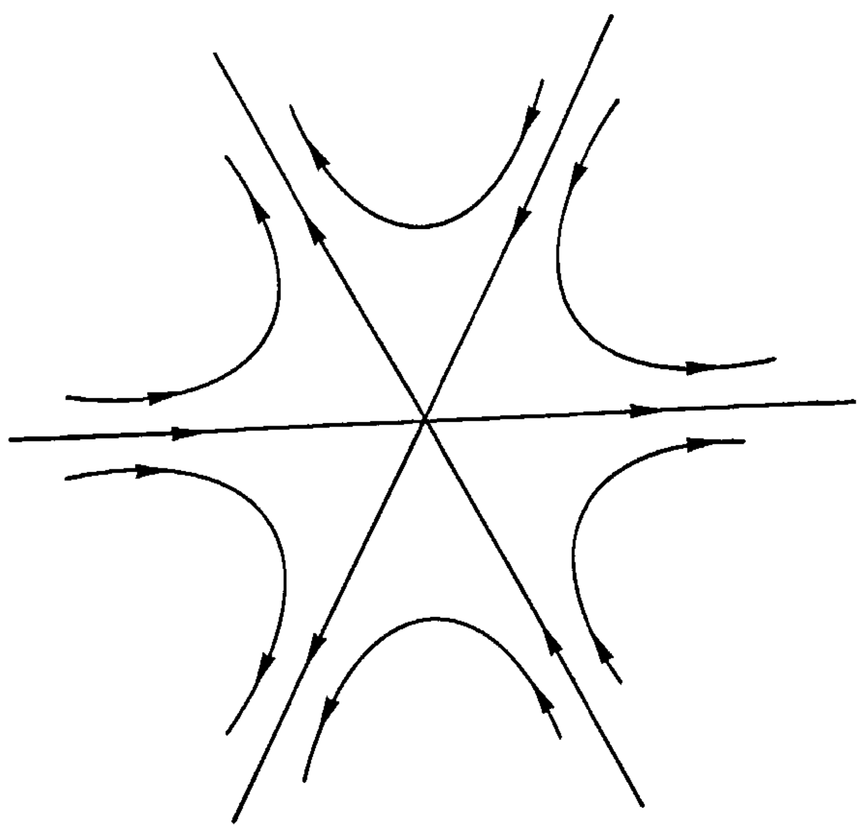

(a)

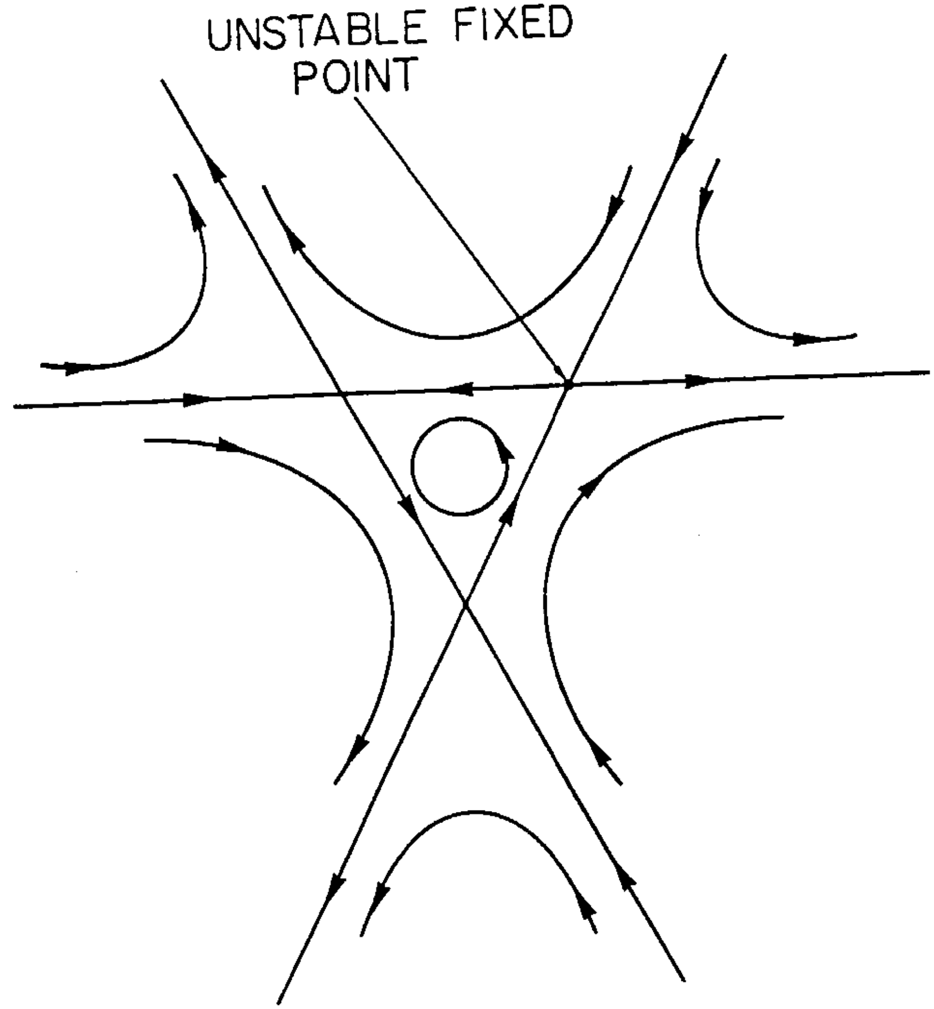

(b)

Figure 9

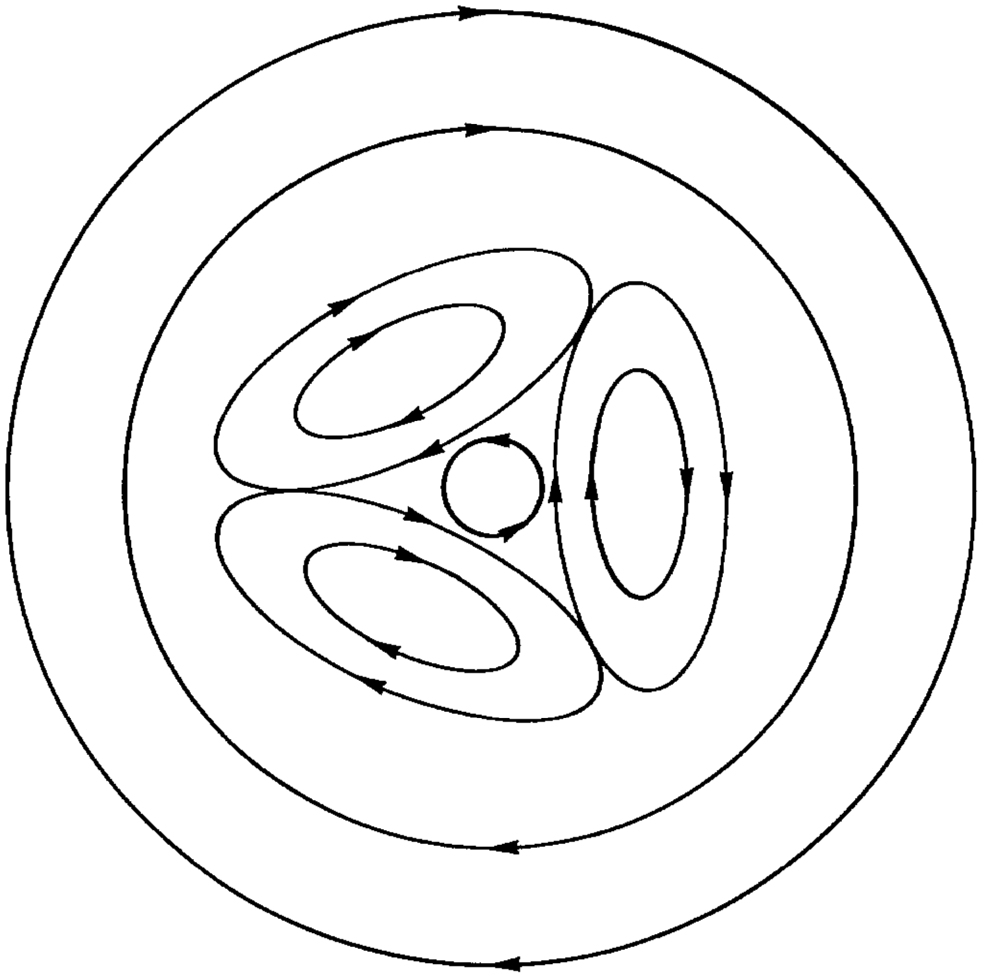

Figure 10

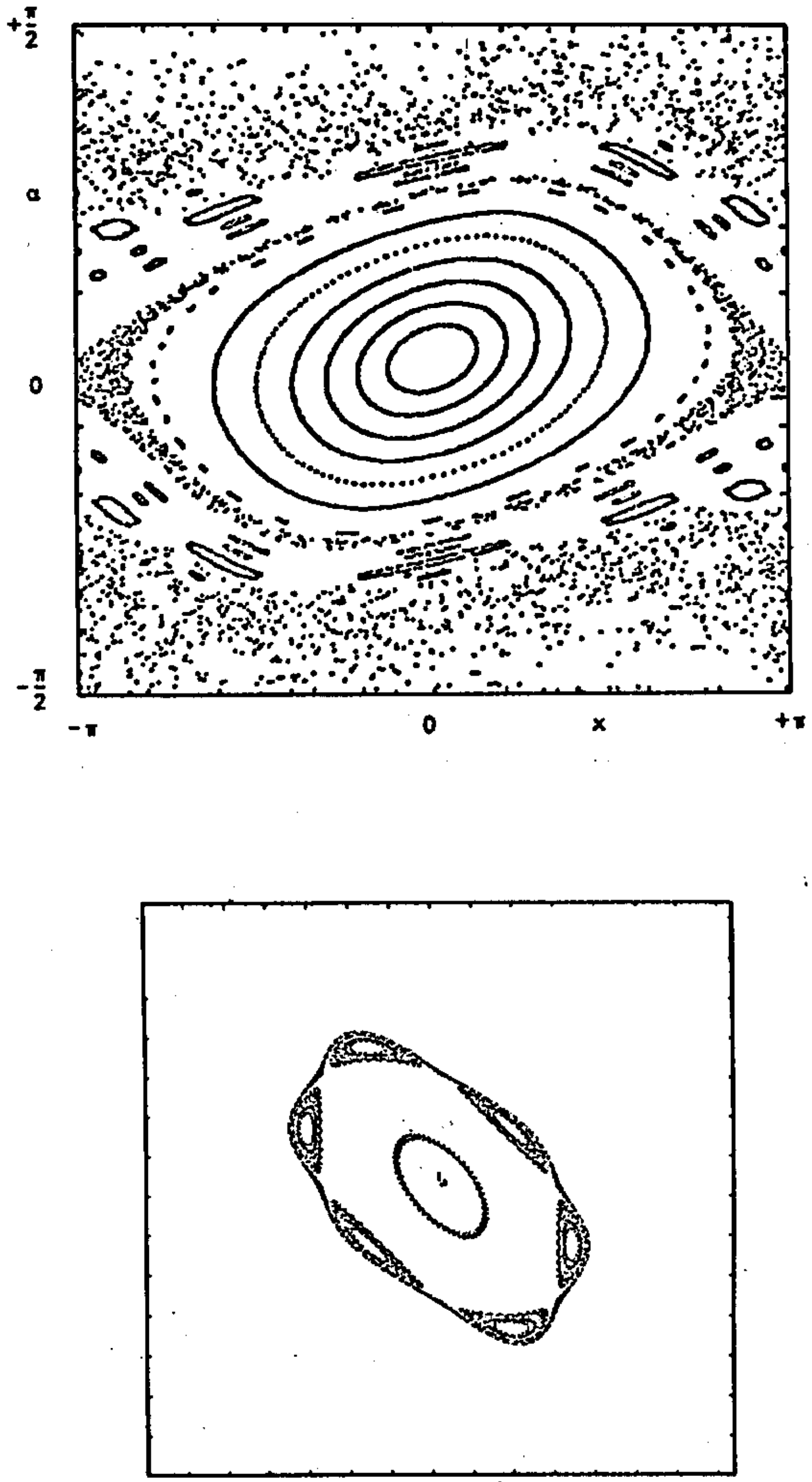

Figure 11

Fig 11

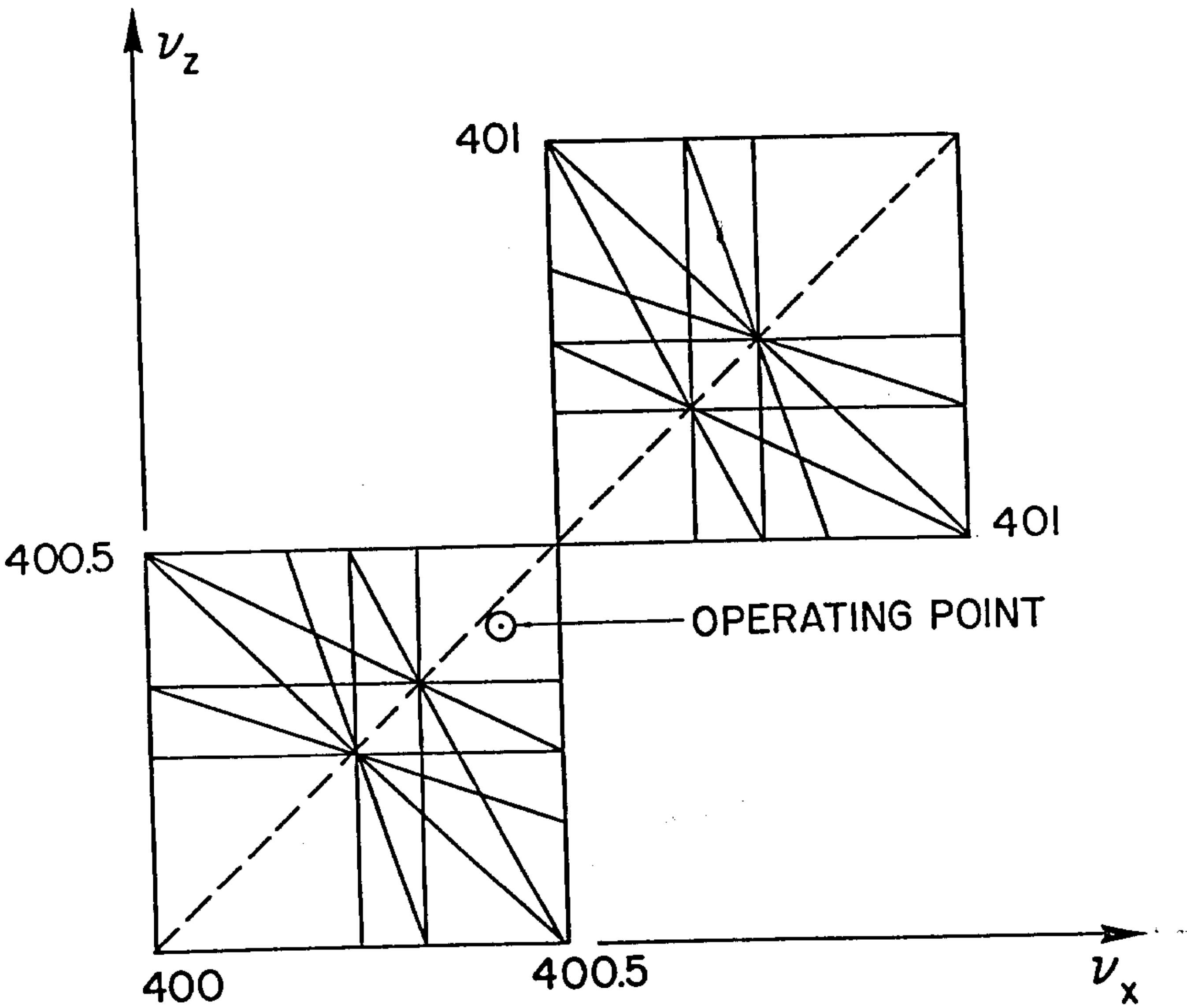

Figure 12

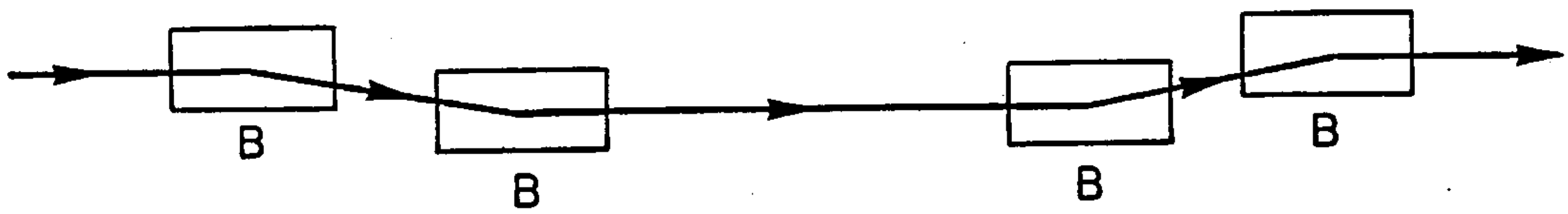

Figure 13

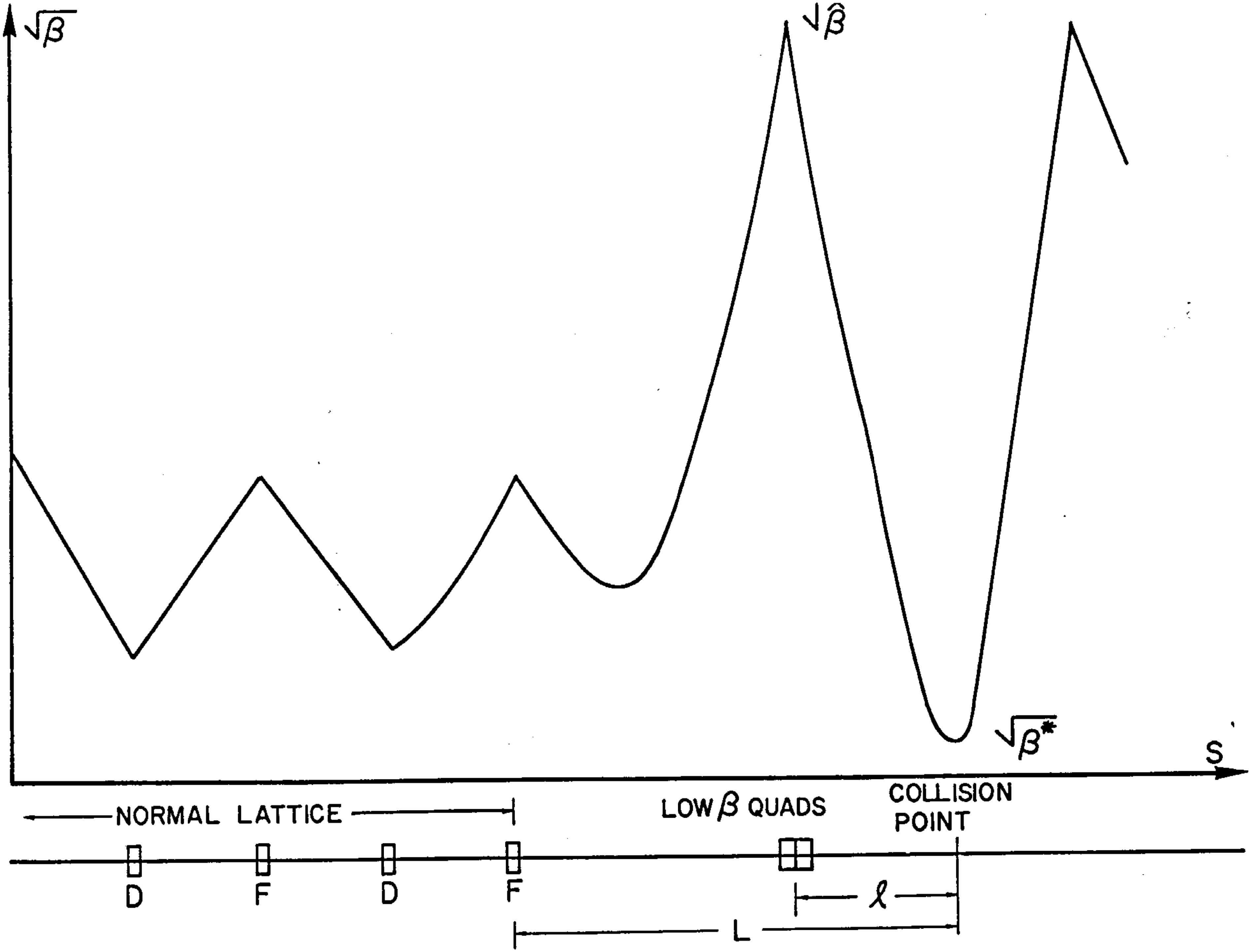
$\sqrt{\beta}$
$\sqrt{\hat{\beta}}$
$\sqrt{\beta^*}$
S
NORMAL LATTICE
LOW β QUADS
COLLISION
POINT
D
F
D
F
ℓ
L

Figure 14

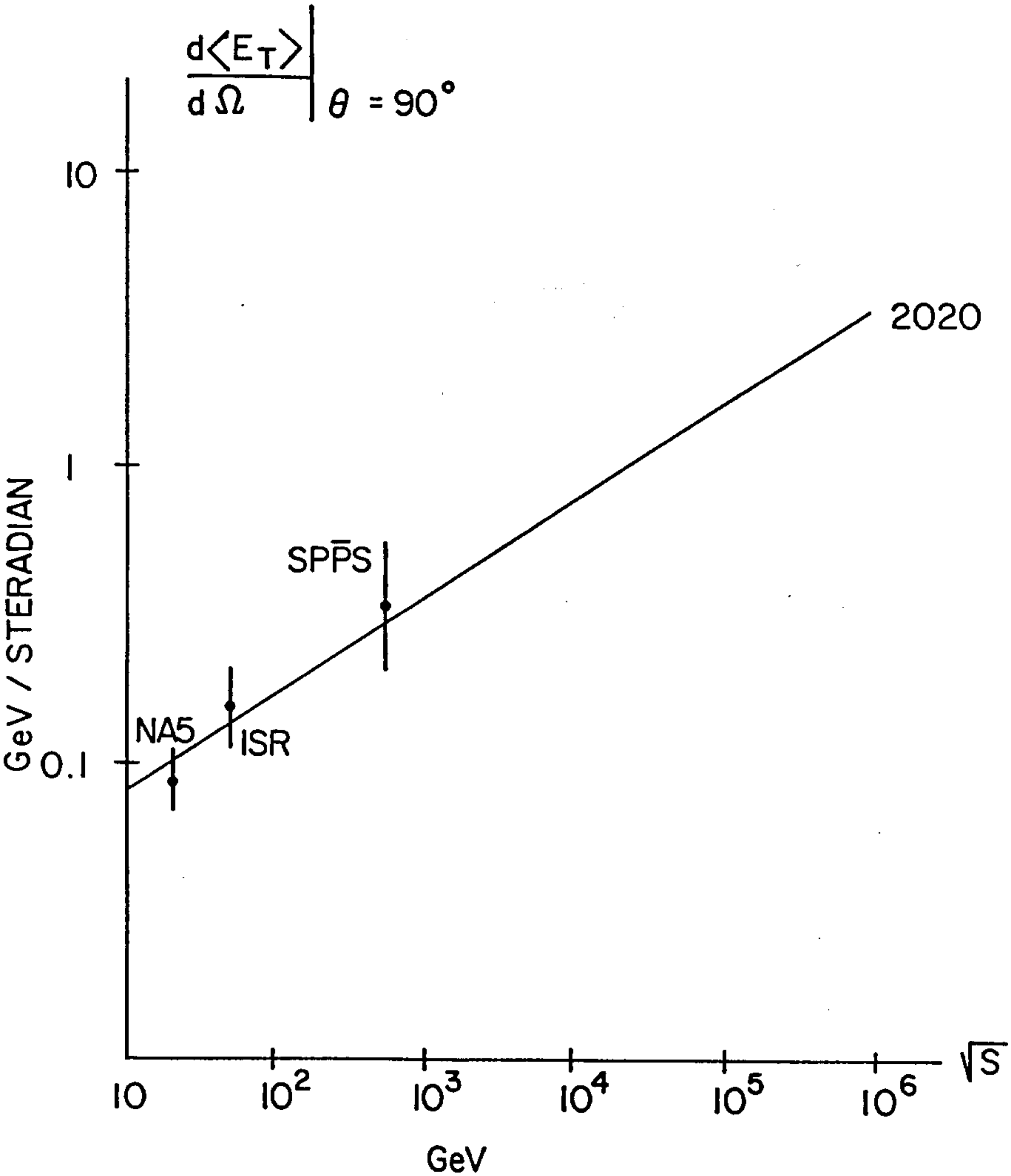

$\left.\frac{d\langle E_T\rangle}{d\Omega}\right|_{\theta=90°}$
10
1
0.1
GeV / STERADIAN
2020
SPP̄S
ISR
NA5
10
10^2
10^3
10^4
10^5
10^6
$\sqrt{S}$
GeV

Figure 15